Fear in the mind's eye:

Mental imagery can generate and regulate acquired differential fear conditioned reactivity

Steven G. Greening[1,2,3]*, Tae-Ho Lee[4,5], Laurent Grégoire[2,6], Lauryn Burleigh[2], Tyler Robinson[2], Xinrui Jiang[2], Mara Mather[3,5,7], and Jonas Kaplan[8]

[1]Department of Psychology, University of Manitoba, Canada

[2]Department of Psychology, Louisiana State University, USA

[3]Leonard Davis School of Gerontology, University of Southern California, USA

[4]Department of Psychology, Virginia Tech, USA

[5]Department of Psychology, University of Southern California, USA

[6]Department of Psychology and Brain Sciences, Texas A & M, USA

[7]Neuroscience Graduate Program, University of Southern California, USA

[8]Brain and Creativity Institute, Dornsife College of Letters Arts and Sciences, University of Southern California, USA

*Correspondence concerning this article should be addressed to Steven G. Greening (steven.greening@umanitoba.ca), Brain and Cognitive Sciences, Department of Psychology, University of Manitoba, Winnipeg, R3T 2N2 Canada. Tel.: +1 204 474 8259.

ABSTRACT

Mental imagery is an important tool in the cognitive control of emotion. The present study tests the prediction that visual imagery can generate and regulate differential fear conditioning via the activation and prioritization of stimulus representations in early visual cortices. We combined differential fear conditioning with manipulations of viewing and imagining basic visual stimuli in humans. We discovered that mental imagery of a fear-conditioned stimulus compared to imagery of a safe conditioned stimulus generated a significantly greater conditioned response as measured by self-reported fear, the skin conductance response, and right anterior insula activity (experiment 1). Moreover, mental imagery effectively down- and up-regulated the fear conditioned responses (experiment 2). Multivariate classification using the functional magnetic resonance imaging data from retinotopically defined early visual regions revealed significant decoding of the imagined stimuli in V2 and V3 (experiment 1) but significantly reduced decoding in these regions during imagery-based regulation (experiment 2).

KEYWORDS

Fear conditioning; Mental imagery; Emotion regulation; FMRI; MVPA

INTRODUCTION

From fears of monsters under our beds to remembering the 'good times' while dealing with the death of a loved one, mental imagery is central to the cognitive control of emotion (Muris et al. 2003; Holmes and Mathews 2005; Opitz et al. 2015). Modern frameworks for conceptualizing the cognitive control of emotion – specifically emotion generation and emotion regulation – have similarly suggested the importance of mental imagery. Gross (2011) suggests a process model in which internal situations (e.g., imagined objects or situations), in addition to external ones, can produce an emotional response. Likewise, mental imagery has been discussed as a potential factor in both distraction and reappraisal strategies for regulating emotions (Ochsner et al., 2012; Opitz et al., 2015).

Fear (or threat) conditioning is one of the most well-studied paradigms for investigating both the generation (Dunsmoor and Murphy 2015; Fullana et al. 2016) and the regulation (Delgado, Nearing, LeDoux, & Phelps, 2008; Phelps, Delgado, Nearing, & LeDoux, 2004; Raio, Orederu, Palazzolo, Shurick, & Phelps, 2013) of emotional reactivity. In differential fear conditioning a neutral conditioned stimulus (CS+) is paired with an aversive unconditioned stimulus (US), such as a mild shock, while a second conditioned stimulus (CS-) is never paired with the US. Following successful fear conditioning, presentation of the CS+ alone elicits a measurable conditioned response (CR, e.g., self-reported subjective fear; a skin conductance response, SCR; or differential neural activity) compared to the CS-.

While much research in human and non-human animals has emphasized the role of the amygdala in the acquisition of differential fear conditioning (Delgado, Olsson, & Phelps, 2006), a recent meta-analysis of functional magnetic resonance imaging (fMRI) studies found that a network that includes both cortical and subcortical regions but *not* the amygdala is reliably

activated by differential fear conditioning (Fullana et al. 2016). This putative fear network includes bilateral aspects of the anterior insula (aIn), dorsal anterior cingulate cortex (dACC), and dorsomedial prefrontal cortex (dmPFC), ventral striatum, thalamus, and midbrain structures.

Mental imagery also appears to interact with differential fear conditioning. For example, Reddan et al. (2018) found that mental imagery of the auditory CSs could be used to induce extinction learning following differential fear conditioning to auditory tones, as measured using SCR and whole-brain multivariate pattern analysis. In addition, mental imagery of CSs can contribute to (Agren et al. 2017) or facilitate (Grégoire and Greening 2019) the reconsolidation of differential fear conditioning. In the current study, we evaluated whether visually acquired differential conditioning generalizes to imagery of the CSs and whether the mechanisms for imagery generation are consistent with depictive theory of mental imagery.

According to the depictive theory (Pearson et al., 2015), mental imagery is the top-down production of neural representations from memory, which are similar to those produced by perception and is associated with a conscious experience of ‘seeing in the mind’s eye’ (Kosslyn, 1983; Pearson et al., 2015). Consistent with the depictive theory, recent neural evidence from fMRI finds that the content of visual experience is similarly encoded across perception and imagination, since it can be decoded from the early visual cortex using multivariate cross-classification (MVCC; Albers, Kok, Toni, Dijkerman, & de Lange, 2013; Stokes, Thompson, Cusack, & Duncan, 2009). In these studies, a classification model is first trained on the pattern of brain activity in the visual cortex elicited by viewing a set of stimuli and then tested the activity elicited by imagining the same stimuli.

Emotion regulation involves the effortful control of cognition or attention so as to modulate emotional reactivity. This includes both down-regulation (e.g., reducing a negative

response, making it *less* negative) and up-regulation (e.g., enhancing a negative response, making it *more* negative). The effortful down-regulation of differential fear conditioning appears to produce significant down-regulation in self-reported fear (Shurick et al. 2012), SCRs and activity in parts of the fear network, including the aIn (Delgado, Gillis, & Phelps, 2008). Delgado et al. (2008) appears to be the only previous research to evaluate the down-regulation of fear conditioning via a strategy involving imagery. During the down-regulate CS+ condition compared to the attend CS+ condition they observed reduced SCR and aIn activity along with increased activation of the dorsolateral prefrontal cortex (dlPFC). The involvement of dlPFC is consistent with broader emotion regulation findings implicating frontoparietal attention control regions in regulation (Buhle et al. 2013). There appears to be no research to date on the up-regulation of differential fear conditioning via mental imagery.

Unresolved in Delgado et al. (2008) and the larger emotion regulation literature is how frontoparietal cortices produce the regulation of brain regions associated with regions of the fear network. While some research indicates that frontoparietal regions operate via connections with the ventromedial prefrontal cortex (Delgado et al., 2008; Johnstone & Reekum, 2007; Wager, Davidson, & Hughes, 2008), other evidence indicates that regulation can occur via the modulation of perceptual areas of the occipitotemporal cortex by attention control processes initiated in frontoparietal cortices (Amting, Greening, & Mitchell, 2010; Greening, Osuch, Williamson, & Mitchell, 2014; Mitchell, Nakic, Fridberg, & Kamel, 2007; Pessoa, McKenna, Gutierrez, & Ungerleider, 2002) via attention control processes as described by the biased-competition theory (Bishop, 2007; Blair & Mitchell, 2009; Greening, Lee, & Mather, 2014).

According to the biased-competition theory (Desimone and Duncan, 1995), when two stimuli compete for representation within a given brain region they do so in a mutually inhibitory

manner. The stimulus that "wins" and becomes preferentially represented is the one that is biased either by stimulus properties or by top-down attention control processes initiated frontoparietal regions (Kastner et al. 1998). Extending this framework to emotion regulation, when we regulate emotional stimuli using distraction or reappraisal, we are prioritizing a representation that compete with the representation of the external emotion elicitor. Combining the depictive theory with the biased-competition theory suggests, therefore, that mental imagery could facilitate emotion regulation via the activation of internally generated representations that compete with external, stimulus-driven, representations.

The present study was designed to address the following two research questions: First, can a differential fear conditioned response be generated through mental imagery, consistent with the mechanisms of the depictive theory of mental imagery? Second, can mental imagery be deployed to regulate differential fear conditioned responding via mechanisms of the depictive theory and the biased-competition model of attention? In order to address these two questions, we conducted a two-visit, two experiment, study that combined differential fear conditioning with manipulations of mental imagery. Both visits involved fMRI combined with SCR recordings and self-reported measures of fear and imagery. A retinotopic functional localizer was used to identify the regions of the early visual cortex (i.e., V1, V2, V3, V4/V3AB) and multivariate cross-class (MVCC; Kaplan, Man, & Greening, 2015) was used to quantify the effects of mental imagery in the visual cortices.

The first question was addressed by testing our first two experimental hypotheses. Hypothesis 1: Imagining a CS+ versus a CS- produces a significant differential response as measured with self-report, SCR, and activation of aspects of the fear network in particular the aIn. Hypothesis 2: Consistent with the depictive theory of imagery, there will be significant

decoding of imagined CS+ versus imagined CS- trials in the early visual cortex. The second question was addressed by testing experimental hypotheses 3 and 4. Hypothesis 3: Imagining the CS- while viewing the CS+ will down-regulate fear response markers (i.e., self-reported fear, SCR, and activity in fear network regions), and imagining the CS+ while viewing the CS- will up-regulate the fear response markers. Hypothesis 4: Consistent with the depictive theory and the biased competition theory, we will observe a significant reduction in decoding accuracy of the CS+ versus CS- in early visual cortex during regulation by imagery (i.e., the down-regulation versus up-regulation conditions) compared to the conditions of viewing the CS+ versus the CS-.

MATERIALS AND METHODS

Participants

Thirteen participants (6 women/7 men, mean age = 24 years, *SD* = 4.87) from the University of Southern California and surrounding community enrolled in this study. None had a history of psychological or neurological disorder. Participants completed two experiments across two days of scanning. One participant dropped out after completing day one (Experiment 1). Thus, Experiment 1 included 13 participants and Experiment 2 included 12. Ten participants performed the second experiment within one week of completing experiment one, while the other two participants completed experiment two 23- and 28-days following experiment one. Our sample size was based on other similar studies that have found positive effects in fear conditioning and emotion regulation (Delgado et al. 2008), fear conditioning and multivariate pattern analysis in the amygdala (Bach et al. 2011), and visual perception and imagery with MVCC (Harrison et al., 2009; Stokes et al., 2009; Vetter et al., 2014). In addition, our experimental design and analysis decisions, which are detailed below, were made alongside our

chosen sample size. All participants provided informed consent and the study was approved by the University of Southern California Institutional Review Board.

Materials

The conditioned stimuli consisted of two Gabor patches (diameter: 8° visual angle; spatial frequency: 2.1 Hz with randomized spatial phase; contrast ratio: 0.75): one oriented 45° from the horizontal (which was referred to as the 'rightward' oriented patch) and one oriented 135° from the horizontal (which was referred to as the 'leftward' oriented patch). Whenever a Gabor was presented it flashed on and off at a rate of 2Hz (1,750ms on, 250ms off) with a random spatial phase to avoid adaptation (Kamitani and Tong 2005). We chose to use Gabor stimuli as previous research demonstrated that they are sensitive to the effects of emotion (Bocanegra and Zeelenberg 2009) and they can be decoded from early visual cortex when being imagined (Albers et al. 2013). The unconditioned stimulus (US) consisted of a 500ms (at 50Hz) mild electric shock delivered to the fingertips of the ring and pinky fingers of the left hand (Lim et al. 2008), administered using E13-22 (Coulbourn Instruments, Allentown, PA), and included MR-compatible leads and electrodes (BIOPAC systems, CA), and a grounded RF filter. The schedule of stimulus presentation was delivered with Psychtoolbox-3 (Brainard 1997; Pelli 1997) in MATLAB (MathWorks, Natick, MA, USA). The auditory instructions were created from www.fromtexttospeech.com (language: US English, Voice: Heather, Speed: medium) and delivered using Sensimetric MRI-compatible Insert Earphones (e.g., Kryklywy, Macpherson, Greening, & Mitchell, 2013).

Design and Procedure

Visit 1, Experiment 1 – Fear generalization to imagined stimuli: The first experiment sought to determine if fear conditioning to a visual object generalizes to instances of mentally imagining the fear conditioned stimulus. This tests the prediction that mental imagery of a CS+ versus CS- generates differential fear response. At the beginning of Experiment 1, electrodes for electrical stimulations were secured and the shock level was adjusted individually to be "unpleasant but not painful" ($M_{intensity}$ = 2.08 mA, *SD* = 0.67, range: 1.10-4.00 mA). Once in the MRI scanner, participants performed three consecutive phases: the habituation phase in which participants only viewed the CSs; the pre-conditioning phase in which participants both viewed and imagined the CSs; and the conditioning phase in which participants viewed and imagined the CSs. The CS+ was paired with shock on 50% of view trials during the conditioning phase. The purpose of the habituation and pre-conditioning phases were to familiarize participants with both the stimuli and the experimental procedures of viewing and imagining the stimuli following the auditory cues.

The habituation phase included six runs composed of five visual presentations of each Gabor patch (in a random order) with no audio, resulting in ten trials per run. Each trial began with a Gabor patch presented for 6.5s and ended with a 12s inter-trial interval (ITI). Participants were instructed to maintain fixation on a center fixation dot (0.5° visual angle), which turned black when a Gabor was present and white during the ITI.

Following habituation, participants completed the pre-conditioning phase which comprised three runs that were each composed of four 'view' trials and four 'imagine' trials of each Gabor patch, for a total of 16 trials per run. The purpose of the pre-conditioning phase was to ensure participants practiced following the instructions including the use of instructed mental imagery. At the beginning of the pre-conditioning phase participants were reminded to maintain

fixation on the center dot, and they were instructed "when the fixation dot turns black this signals the start of a trial and you should listen for and following the instructions; when the fixation dot turns white the trial is over and you can relax and prepare for the next trial". During pre-conditioning, each trial began with an audio instruction (1.5s), which was one of four possibilities: "view right", "view left", "imagine right", "imagine left". Next, either one of the two Gabor patches appeared along with the fixation or the fixation appeared alone for 6.5s. The trial ended with a 12s ITI. The trial presentation order was random.

Most importantly, the final phase of Visit 1 was the fear conditioning phase, which comprised six runs composed of four 'view' trials and two 'imagine' trials of each Gabor patch, for a total of 12 trials per run (see Figures 1a & 1b for a depiction of a view CS+ trial and an imagine CS+ trial, respectively). The general trial structure was identical to the structure of the pre-conditioning phase with the notable exception that one of the two Gabor patches (the order was counterbalanced across participants) was designated as the CS+ and co-terminated with shock on 50% of 'view' CS+ trials. The second Gabor patch, designated as CS-, was never associated with shock. No shock was ever delivered on 'imagine' trials. In addition, the first and the last trial of each run was a 'view' CS-. The second trial of each run was always a 'view' CS+ with shock. All the remaining trials (from trial 3 to 11) were randomized. As with previous research (Delgado et al., 2008; Lim et al., 2008), we excluded the two reinforced CS+ trials of each run from the analyses. We also excluded the first and last CS- trials of each run. This ensured that the number trials per condition included in the analyses were equal and controlled for potentially spurious novelty effects generated on the first trial of each run (Lim et al. 2008). Due to time constraints at the scanner one participant completed 5 habituations runs, 2 pre-

conditioning runs and 3 conditioning runs, while a second participant completed only 2 pre-conditioning runs (all other runs were completed).

Visit 2, Experiment 2 – Regulation of fear conditioning via mental imagery: In the second experiment, we sought to determine if mental imagery can exert an emotion regulation effect such that an internally generated representation competes with an externally generated representation, one of which involves emotional content. Experiment 2 was completed on day two and involved a similar set-up to Experiment 1. First, the electrodes for electrical stimulations were secured and the shock level was adjusted individually to be "unpleasant but not painful" ($M_{intensity}$ = 2.00 mA, *SD* = 0.32, range: 1.40-2.30 mA).

Once in the scanner, participants completed the emotion regulation phase, eight runs that each contained four 'view' trials and two 'regulate' trials of each CS for a total of 12 trials per run. The general task structure was identical to the conditioning phase of Visit 1, except the 'imagine' trials of Visit 1 were replaced with 'regulate' trials (see Figure 3a & 3b for a depiction of a 'view' CS+ and a 'down-regulate' CS+ trial, respectively). The CS+ was the same Gabor across Experiment 1 and Experiment 2 for each participant. The 'view' trials began with the audio instruction to either 'view right' or 'view left', which was followed by the matching Gabor. The 'regulate' trials began with an audio instruction to either "imagine left" or "imagine right". Next, the physical presentation of a Gabor patch began during which participants had to imagine the instructed Gabor patch. While not told explicitly to participants, during 'regulate' trials participants were always instructed to imagine the opposite Gabor from the one presented visually. This produced two 'regulate' conditions: The 'down-regulation' condition during which participants viewed the CS+ while imagining the CS- (vCS+/iCS-); and, the 'up-regulation'

condition during which participants viewed the CS- while imagining the CS+ (vCS-/iCS+). No shock was delivered on 'regulate' trials. Fifty percent of 'view' CS+ trials were reinforced with a co-terminating shock. We used the same approach as in the conditioning phase with regards to trial presentation order, with a 'view' CS- for the first and the last trial of each run, and a 'view' CS+ with shock for the second trial. All the remaining trials (from trial 3 to trial 11) were randomized. Moreover, as with the conditioning phase, all reinforced CS+ trials were excluded from the analyses along with the first and last CS- trials. Due to time constraints at the scanner one participant completed only 5 of the 8 regulation phase runs. During all experimental stages across both days, the participants were attached to the SCR and shock electrodes, and the shock stimulator was set to the 'On' position.

The code associated with the experimental tasks are publicly available at https://osf.io/r87z9/?view_only=5467316afe3940deb10d81792f3bfb52.

Self-report measures

After each experiment, participants provided self-reported evaluations of: 1) the vividness of their mental images on 'imagine' trials, on a 7-point scale ranging from "1 = Non-Existent" to "7 = Very Strong" (e.g., "How vivid was your mental imagery on IMAGINE LEFT trials?"); 2) their effort to form the mental images, on an 7-point scale ranging from "1 = Not At All" to "7 = Very Hard" (e.g., "How hard did you try to form the mental images on IMAGINE RIGHT trials?"); and, 3) their fear of getting shocked on each type of trial, on a 7-point scale ranging from "1 = Not At All" to "7 = Very Much So" (e.g., "How much did you fear the shock on VIEW RIGHT trials?"). For each question participants were asked specifically about one of

the two Gabor patches. Moreover, so as to not bias participants no reference was made to the terms “CS+” or “CS-”.

The behavioral data associated with the experimental tasks are publicly available at https://osf.io/r87z9/?view_only=5467316afe3940deb10d81792f3bfb52.

SCR Methods and Analysis

Consistent with previous research (Greening et al., 2016; Lee et al., 2014; Lee et al., 2018), we measured skin conductance responses (SCRs) during MRI acquisition. The physiological data was recorded at a sampling rate of 1 kHz using BIOPAC’s MP-150 system (BIOPAC System, Goleta, CA, USA). We employed grounded RF filtered MR-compatible leads and MRI-compatible Ag/AgCl electrodes placed on the fingertips of the index and middle fingers of participants’ left hand. Trials including shock delivery were excluded from all analyses, though for the first level fMRI analyses these trials were included as nuisance regressors. Additionally, the first and last trial of each run was a CS- trial which was excluded from the analysis, though they were also included as nuisance regressors for fMRI analyses. This was done to eliminate the potential confounding orienting response to the first trial and to ensure that each condition in the primary analyses included an equal number of trials (Lim et al. 2008). Offline, the SCR data were detrended and smoothed with a median filter over 50 samples to filter out MRI-induced noise and down-sampled to 100 Hz. On a trial-by-trial basis, the SCR epochs were extracted from a time window between 0 and 8 s after CS onset and baseline-corrected by subtracting the mean signal from the one second before CS onset. Next, the peak-from-baseline SCR amplitudes was extracted on a trial-by-trial basis and average over each condition per participant (Lee, Sakaki, Cheng, Velasco, & Mather, 2014). One participant had no detectable

SCR response to the US and was excluded from all SCR analyses, and the SCR equipment malfunctioned during fMRI for two participants during the entire regulation phase. Additional SCR malfunctions occurred for 2 participants on a subset of the data: One participant had no data for one run of the conditioning phase and 2 runs of the regulation phase; the second participant had no data for one run of the regulation phase. The data that we did collect for these two participants were retained and included in the SCR analyses.

MRI Data Acquisition and Analysis:

MRI acquisition: Imaging was performed using a 3T Siemens MAGNETON Trio System with a 32-channel matrix head coil at the Dana and David Dornsife Neuroscience Institute at the University of Southern California. A T1-weighted high-resolution image was acquired on both Visit 1 and Visit 2 of scanning using a three-dimensional magnetization-prepared rapid acquisition gradient (MPRAGE) sequence (TR = 2530 msec, TE = 3.13 msec, flip angle = 10°, 224 × 256 matrix, phase encoding direction right to left). 176 coronal slices covering the entire brain were acquired in sequential order with a voxel resolution of 1mm isotropic.

All functional images (with the exception of the retinotopic mapping) were acquired using a gradient-echo, echo-planar, T2*-weighted pulse sequence (TR = 2000 msec, TE = 25 msec, flip angle = 90°, 64 × 64 matrix, phase encoding direction posterior to anterior). Thirty-eight slices covering the entire brain were acquired with an in-plane voxel resolution of 3.0 × 3.0 and a slice thickness of 3 mm with no gap. Slices were acquired in interleaved ascending order, and each functional run began with the collection of 4 dummy volumes to account for T1 equilibrium effects, which were discarded as part of the later preprocessing steps of data

analyses. The total number of volumes per run, including dummy volumes, varied according to the experimental phase: Habituation (Visit 1) = 98 volumes, Pre-Conditioning (Visit 1) = 85 volumes, Conditioning (Visit 1) = 125 volumes, and Regulation (Visit 2) = 125 volumes.

At the end of Visit 2 we performed two functional retinotopic mapping scans, one for polar angle and one for eccentricity. They were acquired using a gradient-echo, echo-planar, T2*-weighted pulse sequence (TR = 1,200 msec, TE = 30 msec, flip angle = 65°, 78 × 78 matrix, phase encoding direction posterior to anterior). Twenty slices covering the occipital lobe and positioned perpendicular to the calcarine sulcus were acquired with an in-plane voxel resolution of 2.5 × 2.5 and a slice thickness of 2.5 mm with no gap. For each, 254 total volumes were collected including 4 dummy volumes.

We also collected a T2-weighted anatomical scan on Visit 1 (TR = 10,000 ms, TE = 88 ms, flip angle = 120°, 256 × 256 matrix) with 40 transverse slices with a voxel resolution of 0.82 × 0.82 × 3.5 mm. This scan was reviewed by a radiologist to rule out incidental findings and ensure all participants were neurologically normal.

The raw MRI dataset from which the presented findings were generated are available at OpenNeuro.org, using 10.18112/openneuro.ds003425.v1.0.0.

fMRI Preprocessing and Whole-brain Univariate Analysis: FMRI data processing was carried out using FEAT (FMRI Expert Analysis Tool) Version 6.00, part of FSL (FMRIB's Software Library, www.fmrib.ox.ac.uk/fsl). Registration of the functional images to both the high resolution (T1-weighted) structural image and the standard space image was carried out using FLIRT (Jenkinson and Smith 2001; Jenkinson et al. 2002). The following pre-statistics processing was applied: motion correction using MCFLIRT (Jenkinson et al. 2002); slice-timing

correction using Fourier-space time-series phase-shifting; non-brain removal using BET (Smith 2002); spatial smoothing using a Gaussian kernel of FWHM 5mm; grand-mean intensity normalization of the entire 4D dataset by a single multiplicative factor; high-pass temporal filtering (Gaussian-weighted least-squares straight line fitting, with sigma=50.0s). The time-series statistical analysis was carried out using FILM with local autocorrelation correction (Woolrich, Ripley, Brady, & Smith, 2001).

The data were analyzed within the General Linear Model using a multi-level mixed-effects design. At the single-participant level each run was modelled separately. We used a double-gamma hemodynamic response function (HRF) with which each of the conditions of interest (i.e., onset to offset of either viewing or imaging a given Gabor) was convolved. We included a model for the temporal derivative of each condition of interest. We also included several nuisance regressors including six motion correction parameters, and motion censoring regressors for any volume with >0.9mm framewise displacement (Siegel et al. 2014) using the fsl_motion_outliers function. As noted previously we also modelled CS+ reinforced (i.e., shock) trials and the first and last CS- trials as two separate regressors that were not used in higher-level analyses (they were modelled similar to the conditions of interest). A second-level analysis was performed in order to combine contrast estimates from the first level separately for each experimental phase (e.g, the conditioning phase) for each participant. This was completed using a fixed effects model, by forcing the random effects variance to zero in FLAME (FMRIB's Local Analysis of Mixed Effects; Beckmann, Jenkinson, & Smith, 2003; Woolrich, 2008; M. W. Woolrich, Behrens, Beckmann, Jenkinson, & Smith, 2004). Group-level analyses were carried out using FLAME (FMRIB's Local Analysis of Mixed Effects) stage 1 and stage 2 with automatic outlier detection (Beckmann et al., 2003; Woolrich, 2008; Woolrich et al., 2004). The

resulting Z (Gaussianised T/F) statistic images were thresholded using clusters determined by Z>2.3 and a (corrected) cluster significance threshold of P=0.05 (Worsley 2001). All whole-brain unthresholded group-level maps can be viewed at neurovault.org using the link: https://identifiers.org/neurovault.collection:5138.

Neural Overlap Analysis: All references to the neural overlap analysis involved the quantification of the extent of neural overlap between two independent whole-brain group-level maps both of which will have been previously thresholded ($z > 2.3$) and corrected for multiple comparisons (Greening, Finger, & Mitchell, 2011; Man, Kaplan, Damasio, & Meyer, 2012). To quantify the extent of neural overlap when experiencing a differential fear conditioned response to viewed stimuli compared to imagined, we performed a neural overlap analysis on whole-brain group-level maps from the 'view' CS+ > 'view' CS- analysis and the 'imagine' CS+ > 'imagine' CS- analysis (Conditioning phase, Experiment 1).

Context-Dependent Functional Connectivity (Psychophysiological Interaction, PPI): To assess differences in task-specific correlations between a seed region (right aIn) and other areas we performed a psychophysiological interaction (PPI) analysis (O'Reilly et al. 2012) on the data from both the conditioning phase (Visit 1) and the regulation phase (Visit 2) data. In both cases the seed region was produced from the right anterior insula cluster that resulted from the neural overlap analysis of the conditioning phase. This cluster was further restricted by right insula mask of the Harvard-Oxford Cortical atlas. This analysis was performed to test the prediction that modulation of aIn occurred via distinct neural pathways in different conditions.

Specifically, we predicted that whereas 'view' conditions would involve greater connectivity with bottom-up areas such early visual areas and the thalamus, conditions involving imagery ('imagine' CS+ on Visit 1, and 'down-regulate' CS+ on Visit 2) would involve greater connectivity with regions associated with cognitive control and memory such as frontoparietal and medial temporal lobe (MTL) regions, respectively.

At the single-participant (first-level) we ran a general linear model (GLM) that included: our psychological regressor contrasting our two conditions of interest [i.e., Visit 1: ('view' CS+) - ('imagine' CS+)); Visit 2: ('view' CS+) - ('down-regulate' CS+)]; our physiological regressor, which was the time-series of the right aIn extracted from the preprocessed and filtered data supplied to our initial first-level analyses (with no convolution, no temporal derivative and no temporal filtering); and the critical PPI regressor, which is modelled as the interaction between the first two regressor such that the physiological regressor zero centered on the mean (i.e., the 'mean' option) and the psychological regressor is zero centered on the halfway point between the highest and lowest point of the regressor (i.e., the 'center' option). No temporal derivative or temporal filtering was applied to the PPI regressor. Our PPI modelled also included nuisance regressors which included one regressor reflecting the shared variance of the two PPI conditions of interest [Visit 1: ('view' CS+) + ('imagine' CS+)); Visit 2: ('view' CS+) + ('down-regulate' CS+)], all the other conditions, six motion correction parameters, and motion censoring regressors (the same as described in the main level 1 analysis).

Functional Retinotopic Localizer: At the end of day two, all participants completed two functional retinotopic localizer runs: one polar angle, and one eccentricity run (Schwarzkopf et al. 2011; Schwarzkopf and Rees 2013). Both functional localizers involved a flickering

checkerboard (5Hz), the polar angel localizer used a rotating wedge and the eccentricity localizer used an expanded annulus. Each localizer run involved ten cycles, with 25 fMRI volumes per cycle (volumes were 1.2 seconds). The maximum visual angle reach by both the wedge and the annulus was ~8.4 degrees. Participants were instructed to keep their overt attention on the center fixation and to track covertly the flickering checkerboard for randomly presented circular targets. The target had a 5% chance of occurring with each flicker and was presented for 200ms. Participants reported the number of targets they detected at the end of each run orally, however, this information was not record as it was simply to ensure participants were attentive. The primary aim of the retinotopic mapping was to produce individual ROIs of both the bilateral dorsal and ventral aspects of each V1, V2, V3, and V4-V3AB combined (Swisher et al. 2007; Pratte et al. 2013).

Functional retinotopy data was preprocessed using Freesurfer's standard procedures for polar retinotopic mapping, including spatial smoothing with 5mm kernel, resulting in a flattened cortical surface (Engel et al. 1997; Sereno et al. 2001) that was cut along the calcarine sulcus (http://freesurfer.net/fswiki/FreeSurferOccipitalFlattenedPatch). The functional data were overlapped on the flattened map and ROIs were manually traced individually for left and right hemispheres and for the ventral and dorsal aspects of each visual area. After tracing, the surface-based ROIs were converted to volumetric space using Freesurfer then registered to the native space of each participants' functional experimental data using FSL's FNIRT (FMRIB's Nonlinear Image Registration tool) with trilinear interpolation (Smith et al. 2004). The resulting ROIs were thresholded (50%) and visually inspected to ensure no overlap between ROIs.

Multivariate pattern analysis and cross classification in visual cortex: We used MVCC (Kaplan, Man, & Greening, 2015) to evaluate critical aspects of both the conditioning phase and the regulation phase. MVCC involves training a machine learning classifier algorithm in one context or condition and evaluating the performance of the classifier in a different context or condition. If there is significant cross-classification performance this provides evidence of informational similarity between the contexts or conditions. Relevant to the current study, previous research has demonstrated that a classifier trained to discriminate between visual objects such as line patches or letters, can be used to quantify participants degree of visual imagery (Harrison and Tong 2009; Stokes et al. 2009; Albers et al. 2013) or the focus of their visual attention (Kamitani and Tong 2005; Serences et al. 2009; Jehee et al. 2011).

For the conditioning phase, we used MVCC to identify whether when participants were asked to imagine a given Gabor they did so (Figure 2). The outcome of this analysis could provide evidence that generating a decodable signal in early visual cortex is associated with generating a fear conditioned response. For the regulation phase, MVCC allowed us to test the prediction that imagining one stimulus while viewing a second stimulus disrupts the neural representation of each via biased competition. Overall, our prediction is that such competition would result in reduced classifier accuracy during the regulation conditions (during which participants viewed one Gabor while imagining the opposite one) compared to the view conditions.

In the present study, we used the data from our day one habituation phase to train classifiers on each visual cortex ROI for decoding the ‘leftward’ versus ‘rightward’ Gabor patches, during which fear conditioning had not occurred thus ensuring that the classifier was not confounded by any effects of associative learning (See Figure 2a & 5a for a visual depiction of

our MVCC approach in both the conditioning phase and the regulation phase, respectively). Our ROIs were derived from our functional retinotopic localization of V1, V2, V3, and V4-V3AB. All participant specific data and masks used in this analysis were registered to the middle functional volume of the first habituation run.

Preprocessing and first-level modeling of the fMRI data used for MVCC was identical to the univariate analysis with the notable exception that each trial was modelled independently in the first-level GLM. This included smoothing with a 5mm FWHM kernel, which has been shown previously to improve classifier performance (Hendriks et al. 2017). In addition, the data were analyzed in native space, and were not transformed to standard space. These parameters were chosen following an iterative evaluation using leave-one-run-out cross-validation using only the training set data (i.e, the habituation phase data). None of the critical test data, which were the data from the conditioning and regulation phases, were used in parameter optimization.

The MVCC analyses were carried out using PyMVPA (Hanke et al. 2009) on each individual participant, then the within-participant results were aggregated to the group-level for analysis (see below). We used support vector machine (SVM) classification using pyMVPA (Hanke et al. 2009). As is the default in PyMVPA, the SVM hyperparameter 'C' was determined via automatic scaling according to the norm of the data. We used a feature selection step prior to classification for each ROI in which we selected the 120 voxels with the largest positive univariate signal difference (Harrison and Tong 2009; Albers et al. 2013). For each participant/ROI combination we trained the SVM on habituation phase data to classify the presence of the CS+ versus the CS- (or more specifically, the Gabor patch that represented each for a given participant) trial-by-trial. Next, this model was applied to our testing data from the conditioning and regulation phases trial-by-trial. This resulted in two classification accuracy

measurements during each phase. In the conditioning phase, we had the accuracy for both classifying 'view' CS+ versus 'view' CS- and for classifying 'imagine' CS+ versus 'imagine' CS-. In the regulation phase, we had the accuracy for both classifying 'view' CS+ versus 'view' CS- and for classifying 'regulate' CS+ versus 'regulate' CS-. In all instances, chance performance for the classifier was 50%.

For each ROI we estimated a group-level null distribution by combining permutation testing and bootstrapping (Greening, Mitchell, & Smith, 2017; Stelzer, Chen, & Turner, 2013). At the single participant level, we ran 10,000 iterations in which we trained the SVM on data with randomly permuted target labels within the training set (i.e., the habituation data from Visit 1) and tested on the held-out testing data. This produced a null distribution for each participant. Notably, for a given ROI the null distribution used for evaluating classification accuracy on view trials was made comparable to the null used to evaluate imagine or regulation trials by using a seeded random number generator for permuting the target labels of the test set. This is relevant to the between condition analysis below.

Next, to generate a group-level null distribution we used a bootstrapping procedure with 10,000 iterations in which we iteratively generated group mean accuracy estimates by randomly sampling from each participants null distribution with replacement at each iteration (i.e., during each iteration we randomly selected one element from each participant's previously computed null distribution with replacement). Finally, to assess the between condition (e.g., 'view' vs. 'imagine' trials) classification accuracy in a given ROI we compared the accuracy difference between the empirical data to a null distribution of the accuracy differences from the permuted data (10,000 iterations). We also verified that chance performance for all simulation tests was ~50%, which further confirms that there was no systematic bias in our classification.

MVCC analysis of the bilateral amygdala: Although the meta-analytic evidence indicates that there is no reliable univariate response in the amygdala to differential fear conditioning (Fullana et al. 2016), previous research has found that CS+ versus CS- conditions can be decoded in the amygdala using multivariate pattern analysis (Bach et al. 2011). A bilateral amygdala mask from the Harvard-Oxford atlas (thresholded at 50%) was registered to each subject's native space in order to conducted trial-wise within-subject cross classification. Consistent with Bach et al. (2011), 300 voxels with the largest positive univariate signal difference were selected as the features of the model at the subject level. All other MVCC parameters and analysis approaches were as described in the previous section.

To decode CS+ versus CS- during the regulation phase we trained the classifier on data from the day one conditioning phase. In doing so, we first tested the classifier on 'view' CS+ versus 'view' CS- trials during the regulation phase as a positive control. After observing successful cross-classification in this positive control we tested the classifier on 'down-regulate' CS+ versus 'up-regulate' CS- trials. This allowed us to test the prediction that mental imagery regulation would significantly reduce classification accuracy of patterns associated with differential fear conditioning. We also trained a model on the 'view' CS+ versus 'view' CS- trials from the regulation phase (Visit 2) to decode CS+ versus CS- during the conditioning phase (Visit 1). However, the positive control of testing the classifier on 'view' trials during the conditioning phase was not successful (p = .23), thus we were not justified in testing this classifier on imagery trials during acquisition.

Whole-brain multivariate similarity: Although the univariate whole-brain results revealed reliable differences in brain regions associated with fear conditioning and emotion more generally, we also used tool for conducting a more formal reverse inference to further interpret our results. We use the Picture Induced Negative Emotion Signature (PINES) to estimate participants degree of negative affect for each condition from whole-brain data. PINES is a multivariate sparse regression model that was validated using a variety of pictures ranging from neutral to negative in emotional valence (Chang et al. 2015). The PINES model was downloaded from https://neurovault.org/collections/306/. These analyses were carried out on participants second-level data for each condition. We computed a standardized pattern response for each condition per participant based on the spatial correlation between averaged standardized PINES and our data. The higher the outputted value the higher the predicted negative affect the participant experienced for a given condition.

RESULTS

Experiment 1 (Visit 1) – Fear generalization to imagined stimuli

Self-reported fear of shock (Figure 1c), imagery vividness and imagery effort

To test the hypothesis that fear conditioning was acquired to viewed stimuli and transferred to imagined stimuli as measured using subjective markers of fear, we ran a repeated measure analysis of variance (ANOVA) on the self-reported fear of shock data with CS-Type (CS+, CS-) and Instruction (view, imagine) as within-participant variables. There was a CS-Type x Instruction interaction, $F(1, 12) = 6.50$, $p = .025$, $\eta_G^2 = .063$, reflecting a greater difference between CS+ and CS- in the view condition, $t(12) = 7.31$, $p < .001$, $d = 2.03$, than in the imagine condition, $t(12) = 5.50$, $p < .001$, $d = 1.53$. This last effect, however, indicates a generalization of

fear conditioning when imagining the CS+ versus the CS-, as measured with self-report. Additionally, a post-hoc comparison revealed significantly greater subjective fear for 'view' CS+ than 'imagine' CS+, $t(12) = 3.18$, $p = .008$, $d = 0.88$. There was also both a significant main effect of CS-Type, $F(1, 12) = 62.91$, $p < .001$, $\eta_G^2 = 0.56$, with higher self-reported fear for CS+ than for CS- irrespective of Instruction, and a significant main effect of Instruction, $F(1, 12) = 7.44$, $p = .017$, $\eta_G^2 = 0.12$, with greater self-reported fear for viewed than for imagined stimuli.

We verified that self-rated effort to form a mental image did not differ significantly between imagine CS+ and imagine CS- ($M = 5.15$, $SD = 1.41$, and $M = 5.46$, $SD = 1.05$, respectively), $t(12) = 1.00$, $p = .337$ (Supplemental Figure 1). Likewise, vividness of mental imagery did not significantly differ between imagine CS+ and imagine CS- ($M = 4.31$, $SD = 1.11$, and $M = 3.69$, $SD = 1.55$, respectively), $t(12) = 1.38$, $p = .193$ (Supplemental Figure 1). This allowed us to rule out both imagery effort and vividness as potential confounds that might explain differences in any physiological or neural differences observed when comparing 'imagine' CS+ to 'imagine' CS-. Additionally, one-sample t-tests for both CS+ imagery vividness, $t(12) = 10.75$, $p < 0.001$, and CS- imagery vividness, $t(12) = 6.27$, $p < 0.001$, confirmed that participants' mental imagery vividness was significantly greater than 'non-existent' (i.e., greater than 1 on the Likert scale).

Electrodermal activity (Figure 1d)

To test the hypothesis that fear conditioning was acquired to viewed stimuli and transferred to imagined stimuli as measured using physiological markers of fear, we ran a similar ANOVA on the SCR. There was a significant main effect of CS-Type, $F(1, 11) = 12.24$, $p = .005$, $\eta_G^2 = .068$, with higher SCR for CS+ than for CS- irrespective of Instruction; there was no significant main effect of Instruction, $F(1, 11) = 1.85$, $p = .2$, and no significant CS-Type x

Instruction interaction, $F(1, 11) = 0.13$, $p = .72$. Subsequent t-tests indicated that SCRs were significantly greater for CS+ than for CS- in the view condition, $t(11) = 2.94$, $p = .007$, one-tailed, $d = 0.85$, and in the imagine condition, $t(11) = 2.05$, $p = .033$, one-tailed, $d = 0.59$ (one-tailed tests were used because we had a specific directional hypothesis regarding SCR and fear conditioning). Also, note that no significant difference was observed between CS+ view and CS+ imagine, $t(11) = 1.08$, $p = .3$, nor between CS- view and CS- imagine, $t(11) = 1.23$, $p = .24$. Together, these results provide partial evidence that fear acquired to viewed stimuli generalizes to imagined stimuli, as measured with SCR.

Brain Imaging (fMRI)

***Differential fear conditioning to viewed percepts (Figure 1e; Table 1)*:** Our fear conditioning manipulation to viewed stimuli produced canonical activation in a network of regions associated with differential fear conditioning (Fullana et al. 2016). Specifically, there was significantly greater signal in parts of bilateral anterior insula, bilateral dACC, right thalamus, right striatum, and right aspects of the midbrain during the 'view' CS+ compared to 'view' CS- condition.

***Differential fear generalization to imagined percepts (Figure 1f)*:** In the critical contrast for experiment one, we observed significantly greater activity in the right aIn, right dlPFC and bilateral inferior parietal lobe during the 'imagine' CS+ compared to the 'imagine' CS- condition (Table 1).

***Interaction of differential visual fear conditioning versus imaginal fear generalization (Supplemental Figure 2; Table 1)*:** This interaction revealed a broad pattern of activation such that differential imaginal fear generalization [('imagine' CS+) – ('imagine' CS-)] was significantly greater than differential visual fear conditioning [('view' CS+) – ('view' CS-)].

This interaction effect was found in several noteworthy regions including bilateral hippocampus, amygdala, and supramarginal gyrus (see Table 1 for full details). On the other hand, no clusters were significantly greater for differential visual fear conditioning [('view' CS+) – ('view' CS-)] compared to differential imaginal fear generalization [('imagine' CS+) – ('imagine' CS-)].

***Contrast of viewing versus imagining the fear conditioned percept (Supplemental Figure 3; Table 1)*:** We performed the contrast of 'view' CS+ versus 'imagine' CS+ to directly assess which regions are differentially recruited when a visual percept generates a fear conditioned response versus when an imagined percept generates one. As one would predict viewing the CS+ produced significantly more activity in bilateral visual cortex, thalamus, and midbrain regions of the brainstem (i.e., bottom-up regions). Conversely, imagining the CS+ produces significantly greater signal in broad parts of bilateral frontoparietal regions and bilateral medial temporal lobe areas including hippocampus and amygdala. This is consistent with the depictive theory and the role of both attention control and memory regions in mental imagery.

***Neural overlap of differential fear conditioning and imagery generalization (Supplemental Figure 4; Table 2)*:** The neural overlap of the thresholded and corrected whole-brain group-level maps from the 'view' CS+ > 'view' CS- analysis and the 'imagine' CS+ > 'imagine' CS- analysis overlap the right aIn and inferior frontal gyrus. This may suggest that the right aIn is an important location for the expression of both stimulus-driven differential fear conditioning ('view' CS+ > 'view' CS-) and imagery-driven differential fear generalization ('imagine' CS+ > 'imagine' CS-).

***PPI, whole-brain (Supplemental Figure 5, Table 3)*:** The PPI analysis focused on the connectivity of the right aIn during 'view' CS+ versus 'imagine' CS+. The right aIn cluster (restricted with an anatomical insula mask) was defined from the "neural overlap of differential

fear conditioning and imagery generalization" (see above) and was used as the seed region for the PPI. This analysis revealed significantly stronger (and positive) functional connectivity during 'imagine' versus 'view' CS+ between right aIn and bilateral aspect of both the MTL and parietal regions, including bilateral amygdala, hippocampus, lateral occipital cortex, angular gyrus, and superior parietal lobe. On the other hand, there were no significant effects for 'view' CS+ stronger than 'imagine' CS+.

Multivariate Cross-Classification in early visual cortex (Figure 2): In order to quantify whether participants followed the imagery instructions, we measured the cross-classification accuracy of models trained to discriminate the CS+ from the CS- using data from the habituation phase and tested the data from the conditioning phase (Figure 2a) for each of our visual cortex ROIs. Not surprisingly, for the 'view' conditions our classification accuracy was significantly above chance for all regions, V1 (acc = 59.38%; $p = .0017$), V2 (acc = 67.36%; $p < .0001$), V3 (acc = 66.67%; $p < .0001$), and V4-V3AB (acc = 61.81%; $p < .0001$). Importantly, we also found significant classification during the 'imagine' conditions in V2 (acc = 56.60%; $p = .0082$), V3 (acc = 60.07%; $p = .0002$), and V4-V3B (acc = 59.38%; $p = .0003$). We also found that classifier accuracy was significantly better for the 'view' conditions compared to the 'imagine' conditions in V1 ($p = .0166$), V2 ($p = .0048$), and V3 ($p = .0495$), though there was no significant difference found in V4-V3AB ($p = .2812$). Overall, these findings provide group-level evidence that participants were able to generate a pattern of activation during mental imagery similar to a pattern of activation generated when viewing the CS+ versus CS- and are consistent with the depictive theory.

Whole-brain Multivariate Regression (PINES): We evaluated the results of the PINES whole-brain pattern correlation using a 2 (CS-type: CS+, CS-) by 2 (Instruction: View, Imagine)

repeated measures ANOVA. This revealed no significant interaction, $F(1, 12) = 0.77$, $p = .40$, $\eta_G^2 = .011$, or main effect of CS-type, $F(1, 12) = 4.19$, $p = .063$, $\eta_G^2 = .026$, though it did produce a main effect of condition, $F(1, 12) = 11.41$, $p = .005$, $\eta_G^2 = .246$, such that a greater pattern correlation was observed for the view trials compared to the imagine trials. This effect may simply reflect the bottom-up visual processing similarities between the view trials, on which an external stimulus present, and the trials used to train the PINES model, which were visual scenes.

Experiment 2 (Visit 2) – Regulation of fear conditioning via mental imagery

Self-reported fear of shock (Figure 3c), imagery vividness and imagery effort

To test the hypothesis that mental imagery can be used to regulate a fear conditioned response as measured using a subjective marker of fear, we ran a repeated-measures ANOVA on the self-reported fear of shock with CS-Type (CS+, CS-) and Instruction ('view', 'regulate') as within-participant variables. Critically, this revealed a CS-Type x Instruction interaction, $F(1, 11) = 72.40$, $p < .001$, $\eta_G^2 = .617$, reflecting significantly more subjective fear for the CS+ versus CS- in the view condition, $t(11) = 8.51$, $p < .001$, $d = 2.46$, and the reverse effect in the regulate condition such that participants reported more fear for the 'up-regulate' (vCS-/iCS+) versus 'down-regulate' (vCS+/iCS-) condition, $t(11) = 3.22$, $p = .008$, $d = 0.93$. Additionally, whereas there was a significant reduction in subjective fear during 'down-regulate' compared to 'view' CS+, $t(11) = -9.916$, $p = .008$, $d = 2.86$, there was a significant increase in fear during 'up-regulate' versus 'view' CS-, $t(11) = 2.245$, $p = .032$, $d = 0.71$. There was also a significant main effect of CS-Type, $F(1, 11) = 29.24$, $p < .001$, $\eta_G^2 = .357$, with higher self-reported fear for CS+ than for CS-, and a significant main effect of Instruction, $F(1, 11) = 33.00$, $p < .001$, $\eta_G^2 = .381$, with greater self-reported fear for viewed than for imagined stimuli. These results suggest that

mental imagery is capable of leading to both the down-regulation of a visual fear conditioned stimulus, and the up-regulation of fear by imagining a CS+ as measured by self-report.

We verified that effort to form a mental image did not differ significantly between imagining the CS+ (i.e., 'up-regulate') and imagining the CS- (i.e., 'down-regulate) during the regulation phase (M = 6.08, SD = 0.90, and M = 5.75, SD = 1.06, respectively), $t(11) = 1.48$, p = .166 (Supplemental Figure 6 – Left). Likewise, vividness of mental imagery was not significantly different when imagining the CS+ versus imagining the CS- (M = 4.83, SD = 1.27, and M = 4.58, SD = 1.31, respectively), $t(11) = 1.15$, p = .275 (Supplemental Figure 6). Additionally, one-sample t-tests for both CS+ imagery vividness, $t(11) = 10.48$, $p < 0.001$, and CS- imagery vividness, $t(11) = 9.47$, $p < 0.001$, confirmed that participants' mental imagery vividness was significantly greater than 'non-existent' (i.e., greater than 1 on the Likert scale).

Electrodermal activity (Figure 3d)

To test the hypothesis that mental imagery can be used to regulate a fear conditioned response as measured using a physiological marker of fear, similar to the self-report analysis we ran an ANOVA on the SCR data. This revealed a CS Type x Instruction interaction, $F(1, 8) = 5.75$, p = .043, η_G^2 = .042. Subsequent t-tests indicated that self-reported fear was significantly greater for CS+ than for CS- in the view condition, $t(8) = 3.19$, p = .013, d = 1.06, but no significant difference between CS+ and CS- was observed in the regulate condition, $t(8) = 0.04$, p = .518. In addition, compared to the 'view' CS+ condition, the 'regulate' CS+ condition (i.e., vCS+/iCS-) had a significantly lower SCR, $t(8) = 3.51$, p = .008, d = 1.17. The ANOVA also revealed both a main effect of CS-Type, $F(1, 8) = 6.62$, p = .033, η_G^2 = .040, with greater SCR for CS+ than for CS-, and a main effect of Instruction, $F(1, 8) = 6.89$, p = .030, η_G^2 = .069, with greater SCR for the 'view' conditions compared to the 'regulate' conditions. Overall, this

provides evidence for the use of mental imagery in the down-regulation of a fear conditioned response but no evidence for the up-regulation of fear as measured with SCR.

Brain imaging (fMRI)

Univariate region-of-interest analysis (right aIn; Figure 3e,f): Using the right aIn mask produced from the "neural overlap of differential fear conditioning and imagery generalization" in Experiment 1, we found that fear-associated reactivity is modulated by mental imagery-based emotion regulation. Specifically, we ran a 2(CS-Type: CS+, CS-) by 2 (Instruction: 'view', 'regulate') repeated measures ANOVA on mean percent signal change extracted from the right aIn. This revealed the key interaction, $F(1, 11) = 22.48$, $p < .001$, $\eta_G^2 = .282$. This interaction was driven by a significant down-regulation of activity from 'view' CS+ to 'regulate' CS+ (vCS+/iCS-), $t(11) = 2.64$, $p = .023$, $d = 0.761$, and a significant up-regulation of activity from 'view' CS- to 'regulate' CS- (vCS-/iCS+), $t(11) = 3.46$, $p = .005$, $d = 0.999$. Furthermore, there was significantly more activation of right aIn when viewing the CS+ compared to viewing the CS-, $t(11) = 3.95$, $p = .002$, $d = 1.104$, and there was more activity when regulating the CS- compared to regulating the CS+, $t(11) = 2.961$, $p = .013$, $d = 0.855$.

***Differential fear conditioning to viewed percepts (Figure S7; Table 4)*:** As with Experiment 1, a whole-brain analysis with Experiment 2 revealed significantly greater activation for 'view' CS+ compared to 'view' CS- in a network of regions associated with fear conditioning (Fullana et al. 2016) including bilateral aIn, dACC, thalamus, and midbrain regions of the brainstem. Conversely, we also found several areas associated with more activity for 'view' CS- versus 'view' CS+ such as left MTL.

Contrast of the 'down-regulation' versus 'up-regulation' of a fear conditioned response: The whole-brain analysis directly comparing the two 'regulate' conditions revealed no

significant differences between the 'down-regulation' (viewing the CS+ while imagining the CS-) versus 'up-regulation' of a fear conditioning (viewing the CS- while imagining the CS+).

Contrast of 'down-regulation' versus 'view' CS+ (Figure 4a; Table 4): The first of two key univariate whole-brain contrasts of the regulation phase compared viewing the CS+ to down-regulation of the CS+ (vCS+/iCS-). This revealed a robust reduction in brain activity across large parts of the fear conditioning network, including the bilateral anterior insula, bilateral ventral striatum, bilateral thalamus, and midbrain aspects of the brainstem putatively including the PAG during down-regulation compared to viewing the CS+. On the other hand, down-regulation compared to viewing the CS+ was associated with greater activation in posterior aspects of the frontoparietal attention networks, specifically bilateral superior parietal lobe. There was also greater activity in aspects of bilateral medial postcentral gyrus and left lateral occipital cortex.

Contrast of 'up-regulation' versus 'view' CS- (Figure 4b; Table 4): The second key univariate whole-brain contrast of the regulation phase compared viewing the CS- to the CS- up-regulation condition (vCS-/iCS+). This revealed an increase in brain activity across some parts of the fear conditioning network, such as the bilateral aIn and bilateral striatum. Additionally, there was greater activation in aspects of frontoparietal attention areas, including bilateral DLPFC, bilateral IFG, and bilateral superior parietal lobe. Conversely, viewing the CS- compared to the up-regulation condition (vCS-/iCS+) was associated with greater activity is regions associated with the default-mode network, such as bilateral ventromedial prefrontal cortex, and bilateral posterior cingulate cortex.

Interaction of Stimulus Type (CS+, CS-) by Instruction (View, Regulate), (Supplemental Figure 8; Table 4): As predicted this interaction revealed significant modulation of several core fear network regions by imagery-based regulation. The general pattern of

activation observed in all regions was a cross-over interaction such that activation was reduced from 'view' CS+ to 'down-regulate' CS+ and enhanced from 'view' CS- to 'up-regulate' CS-. This pattern was observed in bilateral aIn, ventral striatum, and thalamus, and in midbrain aspects of the brainstem including putative parts of the periaqueductal gray (PAG).

PPI, whole-brain (Supplemental Figure 9; Table 5): On the data from the regulation phase we carried out two PPI analyses using the right aIn ROI as the seed, which was from the differential fear conditioning neural overlap analysis [(vCS+ > vCS-) ∩ (iCS+ > iCS-)] performed on the conditioning phase (Visit 1) data. The first PPI analysis compared aIn connectivity during 'down-regulate' CS+ compared to 'view' CS+. This revealed significantly greater functional connectivity between right aIn and right amygdala, insula and IFG during 'down-regulate' CS+ compared to 'view' CS+. There were no significant effects for 'view' CS+ > 'down-regulate' CS+. The second PPI analysis compared aIn connectivity during 'up-regulate' CS- compared to 'view' CS-. This revealed significantly greater functional connectivity between right aIn and bilateral posterior cingulate cortex, precuneus, and medial occipital cortex. There were no significant effects for 'up-regulate' CS- > 'view' CS-.

MVCC in early visual vortex (Figure 5): After Experiment 1 (Conditioning phase) revealed that we could decode the contents of participants' mental imagery, in Experiment 2 we tested the prediction that imagining a stimulus competes with the representation of a stimulus being viewed such that decoding accuracy is reduced. For the 'view' conditions of Experiment 2 our classification accuracy was significantly above chance for V1 (acc = 61.88%; $p < .0001$), V2 (acc = 69.06%; $p < .0001$), and V3 (acc = 67.03%; $p < .0001$), though it was not significantly above chance in V4-V3AB (acc = 53.13%; $p = .0841$). During the 'regulation' conditions, in which one of the two Gabor stimuli is on the screen while participants imagined the opposite

stimulus, we also found above chance classification accuracy (of the stimulus being viewed) for V1 (acc = 61.88%; $p < .0001$), V2 (acc = 58.49%; $p = .0008$), and V3 (acc = 60.42%; $p < .0001$), though not V4-V3AB (acc = 54.27%; $p = .0528$). Importantly, while we observed no significant differences in classification accuracy in V1 ($p = .5069$), we observed significantly reduced classification accuracy when regulating compared to viewing in V2 ($p = .0021$) and V3 ($p = .0368$). Overall, these findings indicate that regulation via mental imagery can affect classification performance within V2 and V3, presumably by disrupting the representation of the viewed stimulus.

***MVCC in the amygdala (Figure 6)*:** Bach et al. (2011) argued that the CS-US associations, and therefore the differential encoding of the CS+ versus the CS-, are sparsely distributed throughout the amygdala, which they demonstrated using multivariate pattern analysis. Although we observed neither evidence of greater amygdala activity for the CS+ relative to the CS- conditions (Experiment 1), nor modulation of amygdala activity during the regulation of fear conditioning (Visit 2) according to our univariate whole-brain analysis, we applied MVCC to test the prediction that mental imagery modulates the representation of CS+ versus CS- (Bach et al. 2011). As a positive control, we first demonstrated that a model trained on 'view' CS+ versus 'view' CS- trials from the conditioning phase (Visit 1) could significantly classify 'view' CS+ versus 'view' CS- trials in the regulation phase (Visit 2) above chance, $p = .0095$. Importantly, when this model was tested on 'down-regulate' CS+ versus 'up-regulate' CS- the classification was not significantly different than chance, $p = .7349$. We also observed significantly greater classification accuracy for the 'view' trials compared to the 'regulate' trials ($p = .0169$). Overall, these findings indicate the mental imagery can disrupt the differential patterns of activity associated with the CS+ and the CS-.

Whole-brain Multivariate Regression (PINES), (Supplemental Figure 10): We evaluated the results of the PINES whole-brain pattern correlation using a 2 (CS Type: CS+, CS-) by 2 (Instruction: View, Regulate) repeated measures ANOVA. Critically, this revealed a significant interaction, $F(1, 11) = 5.95$, $p = .033$, $\eta_G^2 = .079$. Follow-up comparisons indicated that this interaction was driven by significantly greater pattern similarity both for 'view' CS+ compared to 'view' CS-, $t(11) = 2.81$, $p = .02$, and for 'view' CS+ compared to 'down-regulate' CS+, $t(11) = 2.33$, $p = .04$. The ANOVA also revealed a main effect of CS Type, $F(1, 11) = 6.03$, $p = .032$, $\eta_G^2 = .089$. There was no significant main effect of Instruction. Overall, these results provide evidence that down-regulation via mental imagery was sufficient to significantly disrupt a neural pattern associated with negative affect.

DISCUSSION

The current study evaluated the general prediction that mental imagery can be used to generate (or express) and regulate fear conditioned responses. It entailed a two-visit, two experiment, study that combined differential fear conditioning with mental imagery of the conditioned stimuli. Both visits involved fMRI combined with SCR recordings and self-reported measures of fear and imagery. The effects of mental imagery were quantified using MVCC on data from regions of the early visual cortex, which were defined using a retinotopic functional localizer. Specifically, two research questions were considered and four study specific hypotheses, two related to the first research question and two related to the second research question.

Generation of a fear conditioned response via mental imagery

Regarding the first research question, our results from Experiment 1 (Visit 1) indicate that a differential fear conditioned response is generated through mental imagery, consistent with the mechanisms of the depictive theory of mental imagery. Consistent with hypothesis 1 we observed mental imagery of the CS+ versus the CS- produced a significant differential response in self-reported fear of shock, SCR, and activation of the right aIn. This pattern of effects was similar to the pattern observed in our control condition involving the visual presentation of the CS+ and CS- (without reinforcement) with several noteworthy observations. We observed that self-reported fear was significantly greater when viewing compared to imagining the CS+, which indicates that participants experience more fear towards the actual object that was paired with shock. Interestingly, this pattern was not observed with the SCR data in which case there was no interaction effect between the viewed versus imagined stimuli. Future research is required to evaluate whether this lack of a differences is reliable or due to our small sample and the noisy nature of SCR. In the fMRI data, while viewing the CS+ versus CS- produced activation of bilateral aIn and dACC, imagery of the CS+ compared to CS- produced significant activation of the right aIn and more dorsal and posterior aspects of the fear network from Fullana et al. (2016) including bilateral supramarginal gyri in the parietal lobe.

While no studies have evaluated the ability of imagery to generate differential fear conditioning along with the potential underlying neural mechanisms, our findings are consistent with several other areas of research relating to conditioning. For example, recent psychophysiological and fMRI research has demonstrated the potential for imagery of the CS+ to contribute to fear extinction (Koizumi et al. 2016; Reddan et al. 2018) or fear reconsolidation (Agren et al. 2017; Grégoire and Greening 2019). Together with the findings from Experiment 1

of the present study, these previous findings are consistent with the ability of mental imagery to contribute to the formation and expression of differential fear conditioning.

The amygdala was not more active during either view or imagery CS+ trials compared to their respective CS- trials in Experiment 1. This lack of heightened amygdala activity (CS+ > CS-) is consistent with two recent meta-analyses of fMRI studies relating to differential fear conditioning (Fullana et al. 2016) and differential instructed fear conditioning (Mechias et al. 2010), neither of which found reliable amygdala activity. On the other hand, the univariate PPI analysis found significantly greater functional connectivity between the aIn and the amygdala when imagining the CS+ compared to viewing the CS+. This PPI analysis more generally revealed greater connectivity between the aIn and bilateral aspects of the MTL and parietal lobe. Taken together this could reflect the greater memory and attention selection processes required of mental imagery compared to viewing (Pearson et al., 2015).

Using MVCC to test our second hypothesis we found significant decoding during mental imagery trials in V2, V3 and V4-V3AB, though in V2 and V3 the decoding accuracy was greater for viewed than imagined stimuli, which is consistent with previous research (Albers et al., 2013; Harrison & Tong, 2009). Furthermore, these general decoding effects of visual mental imagery along with the significantly more accurate decoding of visually presented stimuli are consistent with the depictive theory of mental imagery, which predicts that mental imagery is a weaker mode of sensory perception compared to externally viewing the same object (Pearson et al., 2015). Also consistent with the depictive theory, compared to viewing the CS+, we observed that imagining the CS+ produced significantly more activity in top-down brain areas associated with memory, memory retrieval, and executive attention (Dijkstra et al., 2017; Kreiman et al., 2000; Pearson et al., 2015). These included bilateral hippocampus and other aspects of the medial

temporal lobe, aspects of inferior parietal lobes, and dorsal frontoparietal areas including superior parietal lobe, and inferior and middle frontal gyri (Supplemental Figure 3). Moreover, our PPI analysis revealed significantly greater functional connectivity between the right anterior insula and bilateral MTL and superior parietal lobes when imagining the CS+ compared to viewing the CS+. Lastly, participants self-reported their mental imagery vividness for both the CS+ and CS-, in which case one-sample t-tests were significantly higher than a rating of "Non-existent" vivid (i.e., 1 on the Likert Scale). This is consistent with mental imagery being associated with the subjective experience of 'seeing in the mind's eye'.

Regulation of a fear conditioned response with mental imagery

Regarding the second research question, our results from Experiment 2 (Visit 2) demonstrated that mental imagery can be deployed to regulate differential fear conditioned responding via mechanisms of the depictive theory and the biased-competition model of attention. In support of Hypothesis 3, imagery of the CS- while viewing the CS+ (i.e., the down-regulate condition) compared with viewing the CS+ significantly reduced self-reported fear, SCR, and activity in the right aIn ROI as well as other aspects of the fear network including bilateral anterior insula/frontal operculum, ventral striatum, thalamus, and midbrain. Moreover, in partial support of Hypothesis 3, imagery of the CS+ while viewing the CS- (i.e., the up-regulate condition) compared to viewing the CS- significantly increased self-reported fear and activity in the right aIn ROI. Imagining the CS+ increased activity in other fear network regions including bilateral anterior insula/frontal operculum, striatum, and thalamus. The only inconsistency with Hypothesis 3 was the lack of SCR up-regulation by imagery of the CS+ while viewing the CS-. The pattern of down-regulation observed in the present study is consistent with similar research on the down-regulation of differential fear conditioning using an imagery-based

strategy (Delgado et al., 2008). Regarding up-regulation, to our knowledge our study is the first to measure the up-regulation of differential conditioning via imagery of the CS+. However, previous research has found that the up-regulation of negative affect in response to viewing negative photos increases self-reported negative affect (Ochsner et al., 2004) and activity in brain areas associated with the fear network including aspects of the anterior insula (Schulze et al. 2011). In addition, while we found no evidence for the up-regulation of the SCR, previous research has found that the up-regulation of negative affect while viewing threat-related images is associated with an increased SCR (Eippert et al. 2007).

Frontoparietal regions are generally associated with the cognitive control of emotion. Consistent with previous findings our study revealed that aspects of the superior parietal lobe were more active during both down- and up-regulation compared to their respective viewing conditions. This observation is consistent with the role of superior aspects of the parietal lobe being involved in aspects of visual mental imagery (Dijkstra et al., 2017; Moen et al., 2020) and emotion regulation via reappraisal and distraction (McRae et al. 2010; Kanske et al. 2011).

As in Experiment 1, there was no univariate increase in amygdala activation when viewing the CS+ compared to the CS- nor was there modulation of the amygdala via imagery during the regulation conditions. Consistent with previous research (Bach et al. 2011; Yin et al. 2018), using MVCC, a model trained to distinguish CS+ from CS- using the pattern of bilateral amygdala activity during Experiment 1 (viewing CS+ vs. view CS-) was able to significantly decode the presence of the visual CS+ versus CS- during Experiment 2. Importantly, this same model was not able to decode the CS+ from the CS- during the regulation conditions despite identical visual stimuli. Overall, these findings indicated that mental imagery can successfully

modulate differential fear conditioning, which is consistent with the results obtained in our measures of fear.

Regarding the fourth and final hypothesis: consistent with both the depictive theory and the biased competition theory, we observed a significant reduction in decoding accuracy of the CS+ versus CS- in V2 and V3 during regulation by imagery (i.e., the down-regulation versus up-regulation conditions) compared to the conditions of viewing the CS+ versus the CS-. These effects were observed along with the commensurate modulation of our three measures of fear as noted above. Our findings are, therefore, consistent with previous findings that observe the regulation of emotional reactivity via frontoparietal attention connections to early perceptual and sensory areas, such as the occipitotemporal areas involved in vision (Bishop, 2008; Blair & Mitchell, 2009; Greening et al., 2014; Ochsner et al., 2012). These findings do not refute the likely presences of anterior regulatory pathways involving the lateral PFC (Delgado et al., 2008; Johnstone & Reekum, 2007; Wager et al., 2008) and its connections to the amygdala and aIn. Rather, they are indicative of additional and complementary regulatory mechanisms involving attention selection (Greening et al., 2014; Harris et al., 2013).

There is, however, debate in the literature regarding how early and in which regions attentional competition associated with the regulation of emotion takes place. While some suggest that it occurs in multimodal areas of the temporal lobe reflecting a late process (Blair & Mitchell, 2009; Ochsner et al., 2012), other have suggested that the effects of competition can also occur in early sensory regions such as early visual cortex (Bishop, 2008; Greening et al., 2014; Greening et al., 2014; Pessoa, 2014). Our results indicate that mental imagery can impact neural representations in the early visual cortices, as early as V2 and V3. This does not imply that competition for the purposes of emotion regulation cannot occur later in information

processing, but future research is required to determine how different factors (e.g., using stimuli such as objects or words) affect where and when competition occurs.

While the emotion regulation manipulation used in the present study is best considered a form of distraction, some forms of cognitive reappraisal rely on facets of mental imagery (Opitz et al. 2015). For example, when reappraisal involves imagining novel aspects to a scene it may operate via mechanisms of mental imagery and biased-competition along the occipitotemporal pathways.

Other considerations

The relatively small sample size might be considered a limitation of the current study. However, across both Experiment 1 and 2 we observed consistent and robust differential conditioned responses such that 'view' CS+ was greater than 'view' CS- for all dependent measures emphasized in the analyses of mental imagery. From Experiments 1 and 2 this included the measures of self-reported fear (Figures 1c & 3c), SCR (Figures 1d & 3d), univariate BOLD response in the fear network including bilateral aIn and dACC (Figures 1e & 3e, and Supplemental Figure 7), and the MVCC decoding in the early visual cortex (V1-V3, Figures 2b & 5b). This also included the amygdala decoding (Figure 6b) and whole-brain multivariate PINES analysis in Experiment 2 (Supplemental Figure 10). Taken together, the robust positive control effects alongside the multiple convergent results from across the dependent measures suggest that the primary results regarding the impact of mental imagery on the generation and regulation of emotion via the depictive and biased competition theories are valid.

Conclusion

Taken together, the results of the present study indicate that mental imagery can be cued to successfully generate and regulate a differential fear conditioned association. Furthermore, the findings from MVCC and the early visual cortex are consistent with the depictive theory of mental imagery when imagining a CS+ versus CS- in the absence of external stimuli. Moreover, the MVCC findings that imagining the opposite CS from the one being viewed can regulate emotional reactivity is consistent with both the depictive and biased-competition theories. More broadly, the findings of the present study also support the potential utility of mental imagery-based techniques in the treatment of psychological illness, from imaginal exposure in post-traumatic stress disorder and phobias (Pearson et al., 2013) to imagery rescripting in depression and anxiety (Holmes and Mathews 2010).

ACKNOWLEDGEMENTS

This work was supported by a University of Southern California Postdoctoral Scholars Research Grant; and a Louisiana Board of Regents – Research Competitiveness Subprogram grant to S.G.G. The authors would like to thank Dr. Sam Schwarzkopf for providing the functional retinotopy localizer scripts. S.G.G. conceived of the study; S.G.G, M.M., J.K. designed the study; S.G.G. and T.H.L acquired the data; Data were analyzed by S.G.G. with contributions from J.K. All authors contributed to the interpretation of the results and contributed to the writing of the manuscript. The authors declare no competing interests. Data availability: The unthresholded brain imaging results from the univariate fMRI analyses can be found hosted on neurovault.org, using https://identifiers.org/neurovault.collection:5138. The behavioural data from the current study are available at https://osf.io/r87z9/?view_only=5467316afe3940deb10d81792f3bfb52. The MRI dataset from which the presented findings were generated are available at OpenNeuro.org, using 10.18112/openneuro.ds003425.v1.0.0. Code availability: The code associated with the experimental tasks are publicly available at https://osf.io/r87z9/?view_only=5467316afe3940deb10d81792f3bfb52. Correspondence concerning this article should be addressed to Steven G. Greening (steven.greening@umanitoba.ca), Brain and Cognitive Sciences, Department of Psychology, University of Manitoba, Winnipeg, R3T 2N2 Canada. Tel.: +1 204 474 8259.

REFERENCES

Agren T, Björkstrand J, Fredrikson M. 2017. Disruption of human fear reconsolidation using imaginal and in vivo extinction. Behav Brain Res. 319:9–15.

Albers AM, Kok P, Toni I, Dijkerman HC, de Lange FP. 2013. Shared Representations for Working Memory and Mental Imagery in Early Visual Cortex. Curr Biol. 23:1427–1431.

Amting JM, Greening SG, Mitchell DGV. 2010. Multiple mechanisms of consciousness: the neural correlates of emotional awareness. J Neurosci. 30:10039–10047.

Bach DR, Weiskopf N, Dolan RJ. 2011. A stable sparse fear memory trace in human amygdala. J Neurosci. 31:9383–9389.

Beckmann CF, Jenkinson M, Smith SM. 2003. General multilevel linear modeling for group analysis in FMRI. Neuroimage. 20:1052–1063.

Bishop S. 2008. Neural mechanisms underlying selective attention to threat. Ann N Y Acad Sci. 152:141–152.

Bishop SJ. 2007. Neurocognitive mechanisms of anxiety: an integrative account. Trends Cogn Sci. 11:307–316.

Blair R, Mitchell D. 2009. Psychopathy, attention and emotion. Psychol Med. 543–555.

Bocanegra BR, Zeelenberg R. 2009. Emotion improves and impairs early vision. Psychol Sci. 20:707–713.

Brainard DH. 1997. The Psychophysics Toolbox. Spat Vis. 10:433–436.

Buhle JT, Silvers J a, Wager TD, Lopez R, Onyemekwu C, Kober H, Weber J, Ochsner KN. 2013. Cognitive Reappraisal of Emotion: A Meta-Analysis of Human Neuroimaging Studies. Cereb cortex. 1–10.

Chang LJ, Gianaros PJ, Manuck SB, Krishnan A, Wager TD. 2015. A Sensitive and Specific Neural Signature for Picture-Induced Negative Affect. PLoS Biol. 13:e1002180.

Delgado M, Nearing K, LeDoux J, Phelps E. 2008. Neural circuitry underlying the regulation of conditioned fear and its relation to extinction. Neuron. 829–838.

Delgado MR, Gillis MM, Phelps E a. 2008. Regulating the expectation of reward via cognitive strategies. Nat Neurosci. 11:880–881.

Delgado MR, Olsson A, Phelps E a. 2006. Extending animal models of fear conditioning to humans. Biol Psychol. 73:39–48.

Dijkstra N, Bosch S, van Gerven MAJ. 2017. Vividness of Visual Imagery Depends on the Neural Overlap with Perception in Visual Areas. J Neurosci. 37:1367–1373.

Dunsmoor JE, Murphy GL. 2015. Categories, concepts, and conditioning: how humans generalize fear. Trends Cogn Sci. 19:73–77.

Eippert F, Veit R, Weiskopf N. 2007. Regulation of emotional responses elicited by threat-related stimuli. Hum Brain Mapp. 423:409–423.

Engel S a., Glover GH, Wandell B a. 1997. Retinotopic organization in human visual cortex and the spatial precision of functional MRI. Cereb Cortex. 7:181–192.

Fullana MA, Harrison BJ, Soriano-Mas C, Vervliet B, Cardoner N, Àvila-Parcet A, Radua J. 2016. Neural signatures of human fear conditioning: An updated and extended meta-analysis of fMRI studies. Mol Psychiatry. 21:500–508.

Greening S, Lee T, Mather M. 2016. Individual Differences in Anticipatory Somatosensory Cortex Activity for Shock is Positively Related with Trait Anxiety and Multisensory Integration. Brain Sci. 6:2.

Greening SG, Finger EC, Mitchell DGV. 2011. Parsing decision making processes in prefrontal

cortex: Response inhibition, overcoming learned avoidance, and reversal learning. Neuroimage. 54:1432–1441.

Greening SG, Lee T-H, Mather M. 2014. A dual process of the cognitive control of emotional significance: implications for emotion regulation and disorders of emotion. Front Hum Neurosci.

Greening SG, Mitchell DG V, Smith FW. 2018. Spatially generalizable representations of facial expressions: Decoding across partial face samples. Cortex. 101:31–43.

Greening SGSG, Osuch E a EA, Williamson PCPC, Mitchell DGVDG V. 2014. The neural correlates of regulating positive and negative emotions in medication-free major depression. Soc Cogn Affect Neurosci. 9.

Grégoire L, Greening SG. 2019. Opening the reconsolidation window using the mind's eye: Extinction training during reconsolidation disrupts fear memory expression following mental imagery reactivation. Cognition. 183:277–281.

Hanke M, Halchenko Y, Sederberg P. 2009. PyMVPA: A Python toolbox for multivariate pattern analysis of fMRI data. Neuroinformatics. 37–53.

Harris A, Hare T, Rangel A. 2013. Temporally dissociable mechanisms of self-control: early attentional filtering versus late value modulation. J Neurosci. 33:18917–18931.

Harrison N, Brydon L, Walker C, Gray MA, Steptoe A, Critchley HD. 2009. Inflammation causes mood changes through alterations in subgenual cingulate activity and mesolimbic connectivity. Biol Psychiatry. 66:407–414.

Harrison S a, Tong F. 2009. Decoding reveals the contents of visual working memory in early visual areas. Nature. 458:632–635.

Hendriks MHA, Daniels N, Pegado F, de Beeck HPO. 2017. The effect of spatial smoothing on

representational similarity in a simple motor paradigm. Front Neurol. 8:1–11.

Holmes EA, Mathews A. 2005. Mental imagery and emotion: A special relationship? Emotion. 5:489–497.

Holmes EA, Mathews A. 2010. Mental imagery in emotion and emotional disorders. Clin Psychol Rev. 30:349–362.

Jehee JFM, Brady DK, Tong F. 2011. Attention improves encoding of task-relevant features in the human visual cortex. J Neurosci. 31:8210–8219.

Jenkinson M, Bannister P, Brady M, Smith S. 2002. Improved Optimization for the Robust and Accurate Linear Registration and Motion Correction of Brain Images. Neuroimage. 17:825–841.

Jenkinson M, Smith S. 2001. A global optimisation method for robust affine registration of brain images. Med Image Anal. 5:143–156.

Johnstone T, Reekum C van. 2007. Failure to regulate: counterproductive recruitment of top-down prefrontal-subcortical circuitry in major depression. J Neurosci. 27:8877–8884.

Kamitani Y, Tong F. 2005. Decoding the visual and subjective contents of the human brain. Nat Neurosci. 8:679–685.

Kanske P, Heissler J, Schönfelder S, Bongers A, Wessa M. 2011. How to regulate emotion? Neural networks for reappraisal and distraction. Cereb cortex. 21:1379–1388.

Kaplan J, Man K, Greening SG. 2015. Multivariate Cross-Classification□: Applying machine learning techniques to characterize abstraction in neural representations. Front Hum Neurosci. 9:1–12.

Kastner S, De Weerd P, Desimone R, Ungerleider LG. 1998. Mechanisms of directed attention in the human extrastriate cortex as revealed by functional MRI. Science. 282:108–111.

Katherine C. Moen, Beck MR, Saltzmann SM, Cowan TM, Burleigh LM, Butler LG, Ramanujam J, Cohen AS, Greening S. 2020. Strengthening spatial reasoning: Elucidating the attentional and neural mechanisms associated with mental rotation skill development. Cogn Res Princ Implic. In Press.

Koizumi A, Amano K, Cortese A, Yoshida W, Seymor B, Kawato M, Lau H. 2016. Fear extinction without fear□: Direct reinforcement of neural activity bypasses the need for conscious exposure. Nat Hum Behav. 1:1–7.

Kosslyn SM. 1983. Ghosts in the mind's machine□: creating and using images in the brain. Norton.

Kreiman G, Koch C, Fried I. 2000. Category-specific visual responses of single neurons in the human medial temporal lobe. Nat Neurosci. 3.

Kryklywy JHJH, Macpherson EAE a, Greening SGSG, Mitchell DGVDG V. 2013. Emotion modulates activity in the "what" but not "where" auditory processing pathway. Neuroimage. 82:295–305.

Lee T-H, Sakaki M, Cheng R, Velasco R, Mather M. 2014. Emotional arousal amplifies the effects of biased competition in the brain. Soc Cogn Affect Neurosci.

Lee TH, Greening SG, Ueno T, Clewett D, Ponzio A, Sakaki M, Mather M. 2018. Arousal increases neural gain via the locus coeruleus-noradrenaline system in younger adults but not in older adults. Nat Hum Behav. 2:356–366.

Lim SL, Padmala S, Pessoa L. 2008. Affective learning modulates spatial competition during low-load attentional conditions. Neuropsychologia. 46:1267–1278.

Man K, Kaplan JT, Damasio A, Meyer K. 2012. Sight and Sound Converge to Form Modality-Invariant Representations in Temporoparietal Cortex. J Neurosci. 32:16629–16636.

McRae K, Hughes B, Chopra S, Gabrieli JDE, Gross JJ, Ochsner K. 2010. The neural bases of distraction and reappraisal. J Cogn Neurosci. 248–262.

Mechias M-LL, Etkin A, Kalisch R. 2010. A meta-analysis of instructed fear studies: Implications for conscious appraisal of threat. Neuroimage. 49:1760–1768.

Mitchell D, Nakic M, Fridberg D, Kamel N. 2007. The impact of processing load on emotion. Neuroimage. 34:1299–1309.

Muris P, Bodden D, Merckelbach H, Ollendick TH, King N. 2003. Fear of the beast: A prospective study on the effects of negative information on childhood fear. Behav Res Ther. 41:195–208.

O'Reilly JX, Woolrich MW, Behrens TEJ, Smith SM, Johansen-Berg H. 2012. Tools of the trade: Psychophysiological interactions and functional connectivity. Soc Cogn Affect Neurosci. 7:604–609.

Ochsner K, Ray R, Cooper J. 2004. For better or for worse: neural systems supporting the cognitive down-and up-regulation of negative emotion. Neuroimage. 23:483–499.

Ochsner KN, Silvers J a, Buhle JT. 2012. Functional imaging studies of emotion regulation: a synthetic review and evolving model of the cognitive control of emotion. Ann N Y Acad Sci. 1251:E1-24.

Opitz PC, Cavanagh SR, Urry HL. 2015. Uninstructed emotion regulation choice in four studies of cognitive reappraisal. Pers Individ Dif. 86:455–464.

Pearson DG, Deeprose C, Wallace-Hadrill SM a, Burnett Heyes S, Holmes E a. 2013. Assessing mental imagery in clinical psychology: a review of imagery measures and a guiding framework. Clin Psychol Rev. 33:1–23.

Pearson J, Naselaris T, Holmes EA, Kosslyn SM. 2015. Mental Imagery: Functional

Mechanisms and Clinical Applications. Trends Cogn Sci. 19:590–602.

Pelli DG. 1997. The VideoToolbox software for visual psychophysics: Transforming numbers into movies. Spat Vis. 10:437–442.

Pessoa L. 2014. Précis of The Cognitive-Emotional Brain. Behav Brain Sci. FirstView:1–66.

Pessoa L, McKenna M, Gutierrez E, Ungerleider LG. 2002. Neural processing of emotional faces requires attention. Proc Natl Acad Sci U S A.

Phelps EA, Delgado M, Nearing K, LeDoux J. 2004. Extinction learning in humans: role of the amygdala and vmPFC. Neuron. 43:897–905.

Pratte MS, Ling S, Swisher JD, Tong F. 2013. How attention extracts objects from noise. J Neurophysiol. 110:1346–1356.

Raio CM, Orederu T a., Palazzolo L, Shurick A a., Phelps E a. 2013. Cognitive emotion regulation fails the stress test. Proc Natl Acad Sci. 110:15139–15144.

Reddan MC, Wager TD, Schiller D. 2018. Attenuating Neural Threat Expression with Imagination. Neuron. 100:994-1005.e4.

Schulze L, Domes G, Krüger A, Berger C, Fleischer M, Prehn K, Schmahl C, Grossmann A, Hauenstein K, Herpertz SC. 2011. Neuronal correlates of cognitive reappraisal in borderline patients with affective instability. Biol Psychiatry. 69:564–573.

Schwarzkopf DS, Rees G. 2013. Subjective Size Perception Depends on Central Visual Cortical Magnification in Human V1. PLoS One. 8:e60550.

Schwarzkopf DS, Song C, Rees G. 2011. The surface area of human V1 predicts the subjective experience of object size. Nat Neurosci. 14:28–30.

Serences JT, Ester EF, Vogel EK, Awh E. 2009. Stimulus-specific delay activity in human primary visual cortex. Psychol Sci. 20:207–214.

Sereno MI, Pitzalis S, Martinez A. 2001. Mapping of contralateral space in retinotopic coordinates by a parietal cortical area in humans. Science. 294:1350–1354.

Shurick AA, Hamilton JR, Harris LT, Roy AK, Gross JJ, Phelps EA. 2012. Durable effects of cognitive restructuring on conditioned fear. Emotion. 12:1393–1397.

Siegel JS, Power JD, Dubis JW, Vogel AC, Church JA, Schlaggar BL, Petersen SE. 2014. Statistical improvements in functional magnetic resonance imaging analyses produced by censoring high-motion data points. Hum Brain Mapp. 35:1981–1996.

Smith SM. 2002. Fast robust automated brain extraction. Hum Brain Mapp. 17:143–155.

Smith SM, Jenkinson M, Woolrich MW, Beckmann CF, Behrens TEJ, Johansen-Berg H, Bannister PR, De Luca M, Drobnjak I, Flitney DE, Niazy RK, Saunders J, Vickers J, Zhang Y, De Stefano N, Brady JM, Matthews PM. 2004. Advances in functional and structural MR image analysis and implementation as FSL. Neuroimage. 23:S208–S219.

Stelzer J, Chen Y, Turner R. 2013. Statistical inference and multiple testing correction in classification-based multi-voxel pattern analysis (MVPA): Random permutations and cluster size control. Neuroimage. 65:69–82.

Stokes M, Thompson R, Cusack R, Duncan J. 2009. Top-down activation of shape-specific population codes in visual cortex during mental imagery. J Neurosci. 29:1565–1572.

Swisher JD, Halko M a, Merabet LB, McMains S a, Somers DC. 2007. Visual topography of human intraparietal sulcus. J Neurosci. 27:5326–5337.

Vetter P, Smith FW, Muckli L. 2014. Decoding Sound and Imagery Content in Early Visual Cortex. Curr Biol. 1–7.

Wager T, Davidson M, Hughes B. 2008. Prefrontal-subcortical pathways mediating successful emotion regulation. Neuron. 1037–1050.

Woolrich M. 2008. Robust group analysis using outlier inference. Neuroimage. 41:286–301.

Woolrich MW, Behrens TEJ, Beckmann CF, Jenkinson M, Smith SM. 2004. Multilevel linear modelling for FMRI group analysis using Bayesian inference. Neuroimage. 21:1732–1747.

Woolrich MW, Ripley BD, Brady M, Smith SM. 2001. Temporal Autocorrelation in Univariate Linear Modeling of FMRI Data. Neuroimage. 14:1370–1386.

Worsley KJ. 2001. Statistical analysis of activation images. In: Jezzard P,, Matthews PM,, Smith SM, editors. Functional Magnetic Resonance Imaging. Oxford University Press. p. 251–270.

Yin S, Liu Y, Petro NM, Keil A, Ding M. 2018. Amygdala adaptation and temporal dynamics of the salience network in conditioned fear: A single-trial fmri study. eNeuro. 5.

TABLES

Table 1: Experiment 1 (Visit 1) – Fear generalization to imagined stimuli

#	k	Brain Region	H	Z	MNI *x*	MNI *y*	MNI *z*
View: CS+ > CS-							
1	1001	Frontal Orbital Cortex, Insular Cortex, Frontal Operculum Cortex, Inferior Frontal Gyrus pars opercularis	R	4.05	50	10	0
2	934	Thalamus, Caudate, Putamen, Brain Stem	R/L	4.30	14	-16	16
3	652	Paracingulate Gyrus, Superior Frontal Gyrus, Paracingulate Gyrus, Supplementary Motor Cortex	R	4.04	2	28	42
4	467	Insular Cortex, Frontal Orbital Cortex, Frontal Operculum Cortex, Inferior Frontal Gyrus pars opercularis	L	3.33	-26	16	-14
View: CS- > CS+							
1	32221	Medial Frontal, Middle Frontal & Superior Frontal Gyrus, Precentral & Postcentral Gyrus, Posterior Cingulate Gyrus, Inferior, Middle & Superior Temporal Gyrus, Angular Gyrus, Lingual Gyrus, Occipital Pole, Lateral Occipital Cortex, Hippocampus, Amygdala	R/L	6.08	-4	-30	62
Imagine: CS+ > CS-							
1	1416	Insular Cortex, Inferior Frontal Gyrus pars opercularis, Frontal Operculum, Middle Frontal Gyrus, Temporal Pole	R	4.03	56	12	6
2	1003	Supramarginal Gyrus, Angular Gyrus, Lateral Occipital Cortex, Parietal Operculum	R	3.82	58	-34	44
3	463	Supramarginal Gyrus	L	3.68	-52	-50	46
Imagine: CS- > CS+							
		n.s.					
Interaction: (View CS+ > CS-) > (Imagine CS+ > CS-)							
		n.s.					
Interaction: (Imagine CS+ > CS) > (View CS+ > CS-)							
1	11338	Precentral & Postcentral Gyrus; Inferior & Middle Temporal Gyrus Angular Gyrus, Lateral Occipital Cortex, Lateral Occipital Cortex, Hippocampus & Amygdala	R/L	4.52	-18	-62	64
2	3331	Inferior, Middle, & Temporal Gyrus, Angular Gyrus, Lateral Occipital Cortex, Occipital Pole, Hippocampus, Amygdala	R	3.77	58	-14	0
3	1739	Superior and Middle Frontal Gyrus, Frontal Pole	L	4.26	-30	22	56
4	1293	Supramarginal Gyrus	R	4.04	64	-12	40
5	811	Frontal Pole	R	3.98	-20	60	18
View CS+ > Imagine CS+							
3	3067	Occipital Pole, Lateral Occipital Cortex, Fusiform Gyrus	L	5.7	-38	-78	-20
2	3041	Occipital Pole, Lateral Occipital Cortex, Fusiform Gyrus, Lingual Gyrus	R	5.92	34	-90	2
1	1645	Thalamus, Brain Stem, Caudate	R/L	4.09	8	-26	-8
Imagine CS+ > View CS+							
1	30236	Frontal Pole, Middle Frontal Gyrus, Inferior Frontal Gyrus, Precentral & Postcentral Gyrus, Inferior, Middle &Superior Temporal Gyrus, Angular Gyrus, Supramarginal Gyrus, Superior Parietal Lobe, Occipital Pole, Latera Occipital Cortex; Hippocampus & Amygdala (L), Brain Stem	R/L	5.73	-14	-28	74
2	3548	Superior Temporal Gyrus posterior division, Inferior, Middle & Temporal Gyrus, Parahippocampal Gyrus, Angular Gyrus; Hippocampus & Amygdala	R	4.35	60	-4	-2
3	2979	Postcentral & Precentral Gyrus, Supramarginal Gyrus, Superior Parietal Lobe, Caudate	R	4.33	56	-4	28
4	504	Lingual Gyrus	R/L	3.78	-12	-70	-10
5	406	Frontal Pole, Paracingulate Gyrus	R/L	3.57	12	52	14

= the number of a cluster, ordered by size; k = the number of contiguous voxels in the cluster; Brain region = regions of local maxima included in the broader cluster. The region names are taken generally from the Harvard Oxford atlas in FSL; H = principal hemisphere of the cluster,

right (R) or left (L); Z = maximum z-value from the cluster within the given brain region; MNI(X,Y,Z) = coordinates of the voxel with the maximum effect in the standardized space of the Montreal Neurological Institute (MNI), represented in units of millimeters (mm).

Table 2: Experiment 1, Conditioning Phase: Neural Overlap

Conjunction				MNI		
Brain Region	H	Z	*k*	*x*	*y*	*z*
View (CS+ > CS-) ∩ Imagine (CS+ > CS-)						
Anterior Insula / Frontal Operculum	R	11.80	304	50	10	0
Inferior Frontal Gyrus	R	8.25	13	52	22	18

H = principal hemisphere of the cluster, right (R) or left (L); Z = maximum z-value of cluster; *k* = number of contiguous voxels in the cluster; MNI(X,Y,Z) = coordinates of the center of gravity in the standardized space of the Montreal Neurological Institute (MNI), represented in units of millimeters (mm).

Table 3: Psychophysiological interaction model with right anterior insula seed during conditioning phase

					MNI		
#	k	Brain Region	H	Z	*x*	*y*	*z*
PPI, right anterior insula seed: CS+ > CS+i							
		none					
PPI, right anterior insula seed: CS+i > CS+							
1	1680	Lateral Occipital Cortex, Angular Gyrus, Middle Temporal Gyrus, Precuneus (R/L)	R	3.3	54	-58	26
2	1635	Lateral Occipital Cortex, Angular Gyrus, Middle Temporal Gyrus, Superior Parietal Lobe	L	3.55	-32	-78	34
3	1070	Inferior and Middle Temporal Gyrus, Parahippocampal Gyrus, Hippocampus, Amygdala	R	3.59	34	-20	-24
4	744	Inferior and Middle Temporal Gyrus, Parahippocampal Gyrus	L	3.45	-60	-42	0
5	603	Middle and Superior Frontal Gyrus	R	3.27	32	26	52
6	270	Superior Parietal Lobe	R	3.48	40	-44	54

= the number of a cluster, ordered by size; k = the number of contiguous voxels in the cluster; Brain region = the region(s) in the broader cluster. The region names are taken from the Harvard Oxford atlas in FSL; H = principal hemisphere of the cluster, right (R) or left (L); Z = maximum z-value from the cluster within the given brain region; MNI(X,Y,Z) = coordinates of the voxel with the maximum effect in the standardized space of the Montreal Neurological Institute (MNI), represented in units of millimeters (mm).

Table 4: Experiment 2 (Visit 2) – Regulation of fear conditioning via mental imagery

					MNI		
#	k	Brain Region	H	Z	*x*	*y*	*z*
View: CS+ > CS-							
1	16941	Insular Cortex, Frontal Operculum, Inferior Frontal Gyrus, Supplementary Motor Cortex, Precentral Gyrus, Anterior Cingulate Gyrus, Caudate, Putamen, Brain Stem	R/L	5.07	-58	10	-2

2	1542	Supramarginal Gyrus	R	6.53	62	-44	30
3	1055	Supramarginal Gyrus	L	4.54	-64	-38	28
4	548	Frontal Pole	R	3.82	40	44	32
5	487	Temp. Occipital Fusiform	L	3.97	-34	-66	-24
View: CS- > CS+							
1	480	Postcentral Gyrus	L	3.73	-36	-32	68
2	447	Lateral Occipital Cortex	L	4.25	-38	-76	44
3	408	Hippocampus, Parahippocampal Gyrus	L	4.22	-28	-42	-10
Regulate: (view CS+, imagine CS-) > (view CS-, imagine CS+)							
		none					
Regulate: (view CS-, imagine CS+) > (view CS+, imagine CS-)							
		none					
Down-Regulation (view CS+, imagine CS-) > View CS+							
1	913	Lateral Occipital Cortex superior division	L	5.92	-20	-70	62
2	744	Lateral Occipital Cortex superior division	L	4.35	-26	-72	34
3	551	Precentral Gyrus	R/L	4.94	6	-30	70
4	457	Lateral Occipital Cortex superior division	R	4.67	30	-64	58
View CS+ > Down-Regulation (view CS+, imagine CS-)							
1	4121	Insula, Supramarginal Gyrus, Caudate, Putamen, Thalamus (R/L), Brain Stem	R	4.22	12	0	14
2	1591	Insula, Caudate, Putamen	L	3.8	-30	20	-4
3	1089	Cingulate Gyrus, Superior Frontal Gyrus	R	3.9	4	18	32
4	531	Frontal Pole	R	3.61	26	52	-10
5	516	Supramarginal Gyrus	L	3.79	-64	-30	28
Up-Regulation (view CS-, imagine CS+) > View CS-							
1	9655	Insula, Inferior Frontal Gyrus, Middle Frontal Gyrus, Frontal Pole, Putamen, Caudate, Anterior Cingulate Gyrus (R/L), Supplementary Motor Cortex (R/L), Precentral Gyrus (R/L)	R	4.82	48	12	6
2	3997	Supramarginal Gyrus, Superior Parietal Lobe, Lateral Occipital Cortex superior division, Middle Temporal Gyrus	L	4.23	-34	-64	58
3	3855	Insula, Inferior Frontal Gyrus, Middle Frontal Gyrus, Frontal Pole, Putamen, Caudate	L	3.96	-26	24	6
4	3189	Supramarginal Gyrus, Superior Parietal Lobe, Lateral Occipital Cortex superior division, Middle Temporal Gyrus	R	4.63	36	-44	52
5	422	Temp. Occipital Fusiform, Cerebellum	R	3.51	38	-66	-24
6	396	Occipital Fusiform Gyrus, Cerebellum	L	3.61	-30	-56	-30
View CS- > Up-Regulation (view CS-, imagine CS+)							
1	1206	Frontal Pole, Frontal Medial Cortex, Cingulate Gyrus anterior division, Superior Frontal Gyrus, Paracingulate Gyrus	R	3.73	4	48	-10
2	1034	Cingulate Gyrus posterior division, Precuneus	R	3.9	-4	-52	10
3	410	Middle & Superior Frontal Gyrus	R	3.71	24	28	50
Interaction: View (view CS+ > view CS-) > Regulate ((view CS+, imagine CS-) > (view CS-, imagine CS+))							
1	9494	Insula, Inferior Frontal Gyrus, Precentral Gyrus, Putamen, Caudate, Thalamus, Brain Stem, Anterior Cingulate Gyrus (R/L), Supplementary Motor Cortex (R/L)	R	5.75	38	4	62
2	5101	Insula, Inferior Frontal Gyrus, Precentral Gyrus, Putamen, Caudate, Thalamus, Brain Stem	L	4.58	-20	4	2
3	1231	Supramarginal Gyrus	R	3.95	44	-34	26
4	893	Supramarginal Gyrus	L	3.93	-64	-16	18
5	543	Precentral Gyrus	L	3.83	-54	-2	48
6	487	Frontal Pole, Middle Frontal Gyrus	R	3.7	46	30	12
Interaction: Regulate ((view CS+, imagine CS-) > (view CS-, imagine CS+)) > View (view CS+ > view CS-)							
		none					

= the number of a cluster, ordered by size; k = the number of contiguous voxels in the cluster; Brain region = the region of local maxima included in the broader cluster. The region names are taken from the Harvard Oxford atlas in FSL; H = principal hemisphere of the cluster, right (R) or left (L); Z = maximum z-value from the cluster within the given brain region; # = number of voxels from the cluster inside the given brain region. Regions with less than 5 voxels in the cluster are not reported, except if it is the only cortical region identified in the cluster;

MNI(X,Y,Z) = coordinates of the voxel with the maximum effect in the standardized space of the Montreal Neurological Institute (MNI), represented in units of millimeters (mm).

Table 5: Psychophysiological interaction model with right anterior insula seed during regulation phase

					MNI		
#	k	Brain Region	H	Z	*x*	*y*	*z*
Down-Regulate (vCS+/iCS-) > View CS+							
1	663	Amygdala, Putamen, Insula	R	3.41	14	2	-14
2	395	Angular Gyrus, Middle Temporal Gyrus	L	3.27	-60	-42	0
3	355	Lateral Occipital Cortex superior division	R	3.15	10	-66	64
4	350	Frontal Pole, Inferior Frontal Gyrus	R	3.37	38	40	-8
View CS+ > Down-Regulate (vCS+/iCS-)							
		none					
Up-Regulate (vCS-/iCS+) > View CS-							
		none					
View CS- > Up-Regulate (vCS-/iCS+)							
1	534	Precuneus, Posterior Cingulate Gyrus	R/L	3.43	-2	-54	30
2	388	Supracalcarine Cortex, Intracalcarine Cortex	R/L	3.29	8	-84	4

= the number of a cluster, ordered by size; k = the number of contiguous voxels in the cluster; Brain region = the region of local maxima included in the broader cluster. The region names are taken from the Harvard Oxford atlas in FSL; H = principal hemisphere of the cluster, right (R) or left (L); Z = maximum z-value from the cluster within the given brain region; MNI(X,Y,Z) = coordinates of the voxel with the maximum effect in the standardized space of the Montreal Neurological Institute (MNI), represented in units of millimeters (mm).

CAPTIONS TO FIGURES

FIGURE 1. The trial sequence from Experiment 1 for (a) a 'view' CS+ trial and (b) an 'imagine' CS+ trial. c) Self-reported fear of shock; and d) SCR results. While Red bars denoted the CS+ and Blue bars represented the CS-. Error-bars represent 95% confidence intervals. Black dots represent individual data points. For the self-reported fear of shock data, the size of the circle represents the number of participants that endorsed a given response. Activation maps for (e) 'view' CS+ > 'view' CS-. Activation maps for (f) 'imagine' CS+ > 'imagine' CS-.

FIGURE 2. MVCC in early visual cortex during the conditioning phase (experiment 1). a) A graphical representation of the MVCC training and testing scheme. The lightening bold denotes the CS+ but the MVCC analysis excluded trials in which shock was delivered. b) results of the MVCC classification of view trials (vCS+ vs. vCS-; dark-gray bars) and imagine conditions (light-gray bars) in V1 (top-left), V2 (top-right), V3 (bottom-left), and V4-V3AB (bottom-right). The horizontal line represents chance (50%), and the black dots represent how many participants had a given classifier accuracy.

FIGURE 3. Depiction of the trial sequence for experiment 2 for (a) a 'view' CS+ trial, and (b) an 'down-regulate' CS+ trial in which participants are cued to imagine the CS- while viewing the CS+. c) Self-reported fear of shock and (d) SCR results. (e) BOLD response for the right anterior insula during experiment 2, emotion regulation phase. (f) The right anterior insula mask was derived from the neural overlap analysis from experiment 1 restricted to the insula. In general, 'Regulate' indicates that participants were cued to imagine the opposite stimulus to the one being

viewed. Error-bars represent 95% confidence intervals. Black dots the number of participants that shared a given value in the dependent measure.

FIGURE 4. Results from the whole-brain analysis of the emotion regulation phase (experiment 2). a) Results comparing the 'down-regulate' CS+ (red-yellow) condition to the 'view' CS+ (blue-light blue) condition. The 'down-regulate' CS+ had participants imagine the CS- while viewing the CS+. b) Results comparing the 'up-regulate' CS- (red-yellow) condition to the 'view' CS- (blue-light blue) condition. The 'up-regulate' CS- had participants imagine the CS+ while viewing the CS-.

FIGURE 5. MVCC in early visual cortex during the emotion regulation phase (experiment 2). a) A graphical representation of the MVCC training and testing scheme. The lightening bold denotes the CS+ though the MVCC analysis excluded trials with shock. b) Results of the MVCC classification of view trials (vCS+ vs. vCS-; dark-gray bars) and regulate conditions ('down-regulate' (vCS+/iCS-) vs. 'up-regulate' (vCS-/iCS+); light-gray bars) in V1 (bottom-left), V2 (bottom-middle), V3 (bottom-right). The horizontal line represents chance (50%), and the black dots represent how many participants had a given classifier accuracy.

FIGURE 6. MVCC in the amygdala during the emotion regulation phase (experiment 2). a) A graphical representation of the MVCC training and testing scheme. The lightening bold denotes the CS+. b) Results of the MVCC classification of view trials (vCS+ vs. vCS-; dark-gray bars) and regulate conditions ('down-regulate' (vCS+/iCS-) vs. 'up-regulate' (vCS-/iCS+); light-gray

bars) in bilateral amygdala. The horizontal line represents chance (50%), and the black dots represent how many participants had a given classifier accuracy.

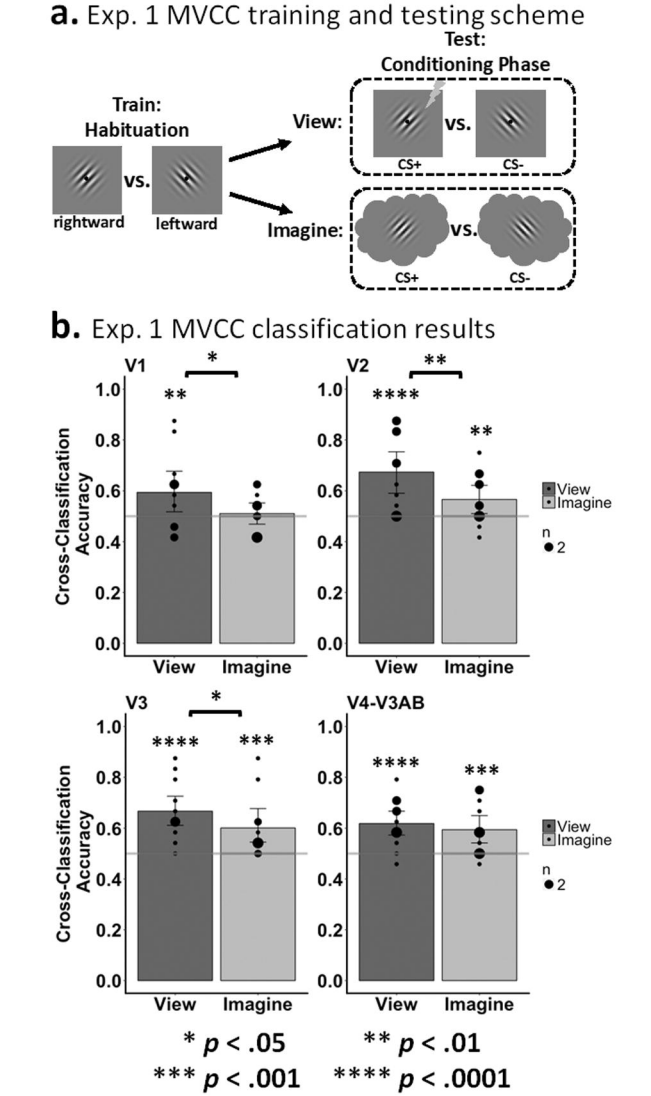
a. Exp. 1 MVCC training and testing scheme
Test:
Conditioning Phase
Train:
Habituation
View:
vs.
CS+
CS-
rightward
leftward
Imagine:
b. Exp. 1 MVCC classification results
V1
V2
V3
V4-V3AB
Cross-Classification Accuracy
View
Imagine
n
2
* p < .05
** p < .01
*** p < .001
**** p < .0001

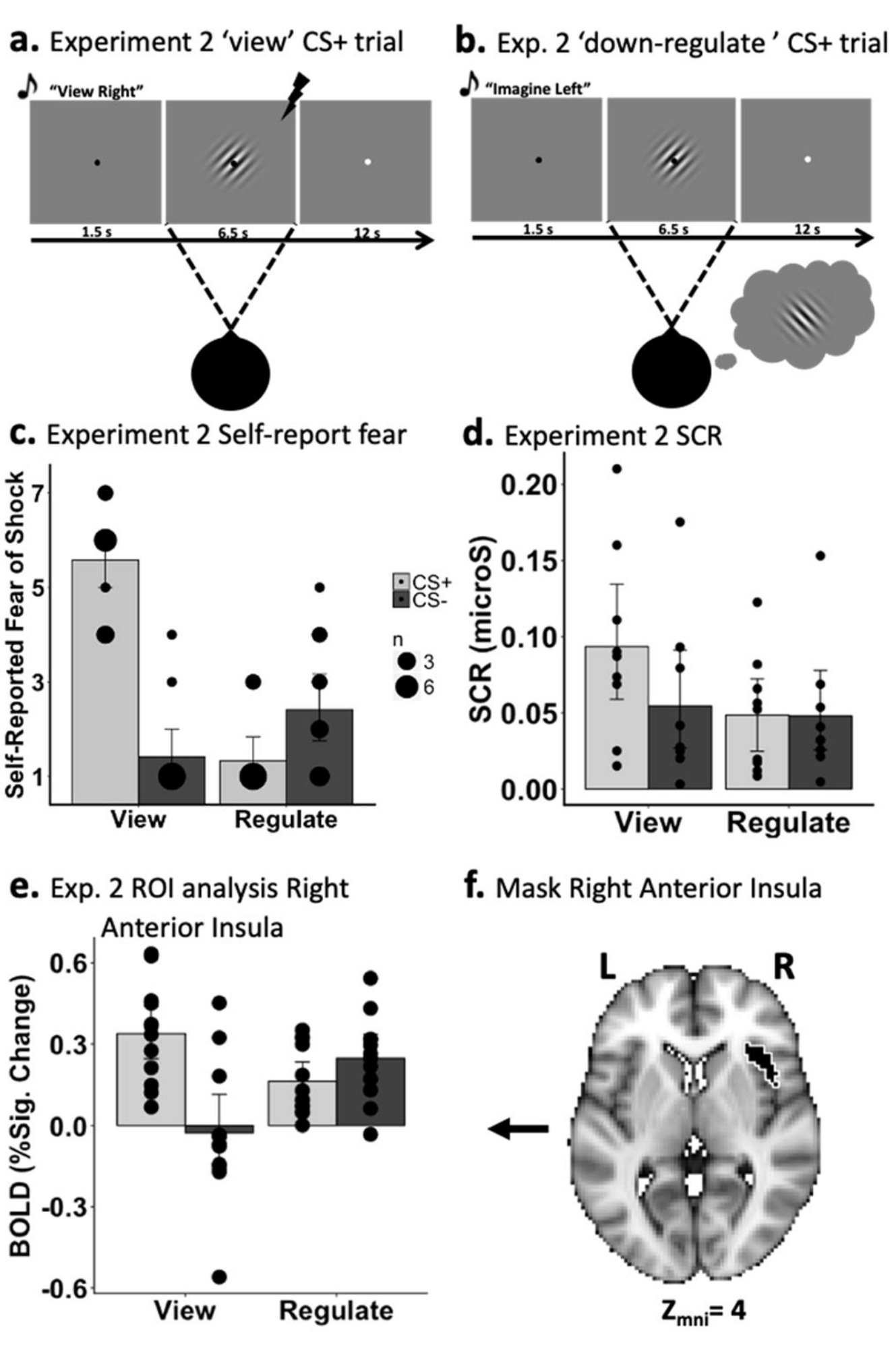
a. Experiment 2 'view' CS+ trial
"View Right"
1.5 s
6.5 s
12 s
b. Exp. 2 'down-regulate ' CS+ trial
"Imagine Left"
1.5 s
6.5 s
12 s
c. Experiment 2 Self-report fear
Self-Reported Fear of Shock
7
5
3
1
CS+
CS-
n
3
6
View
Regulate
d. Experiment 2 SCR
SCR (microS)
0.20
0.15
0.10
0.05
0.00
View
Regulate
e. Exp. 2 ROI analysis Right Anterior Insula
BOLD (%Sig. Change)
0.6
0.3
0.0
-0.3
-0.6
View
Regulate
f. Mask Right Anterior Insula
L
R
Z_mni= 4

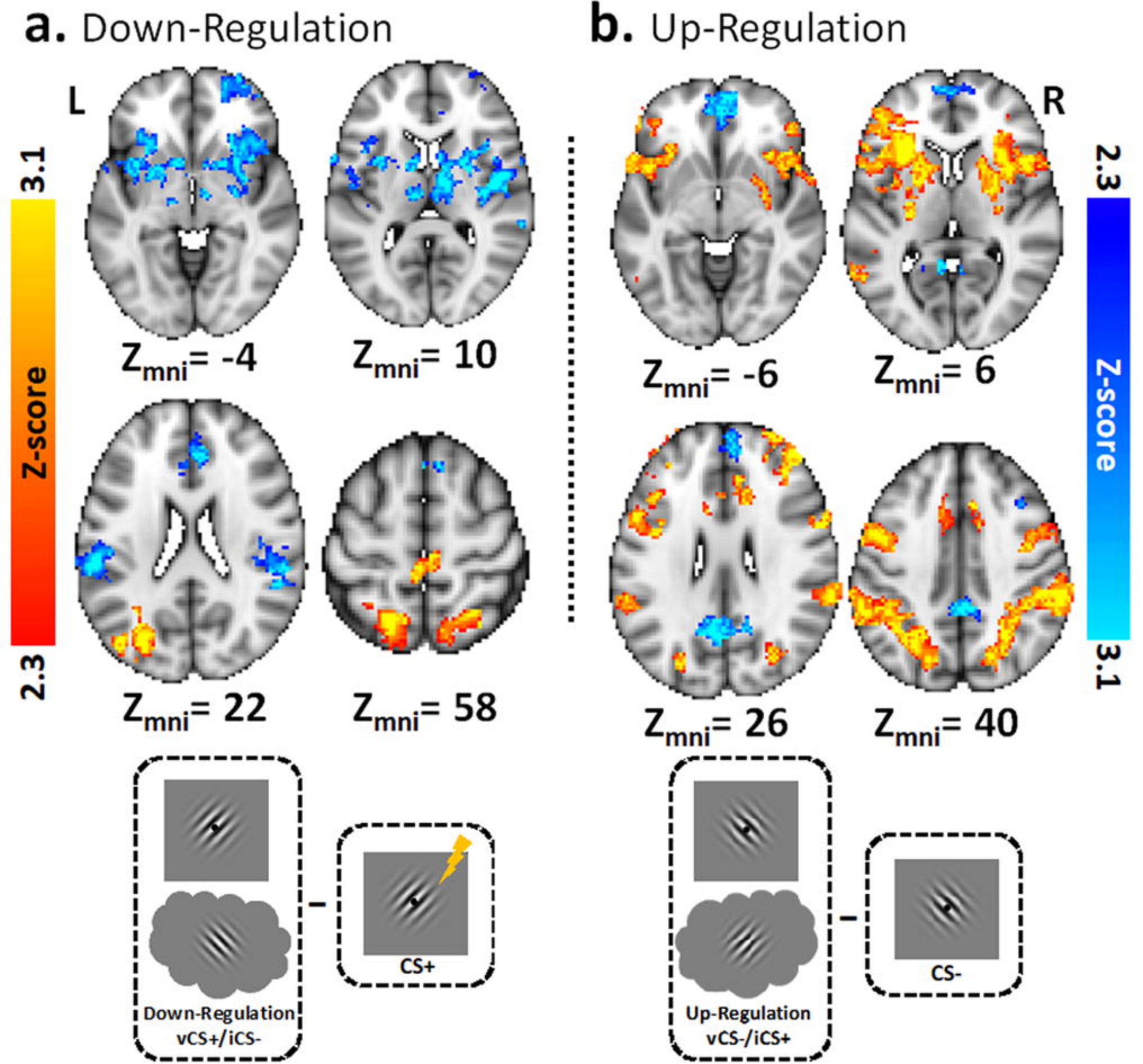
a. Down-Regulation
b. Up-Regulation
L
R
3.1
Z-score
2.3
2.3
Z-score
3.1
Zmni= -4
Zmni= 10
Zmni= -6
Zmni= 6
Zmni= 22
Zmni= 58
Zmni= 26
Zmni= 40
Down-Regulation
vCS+/iCS-
CS+
Up-Regulation
vCS-/iCS+
CS-

a. Exp. 2 visual cortex MVCC training and testing scheme

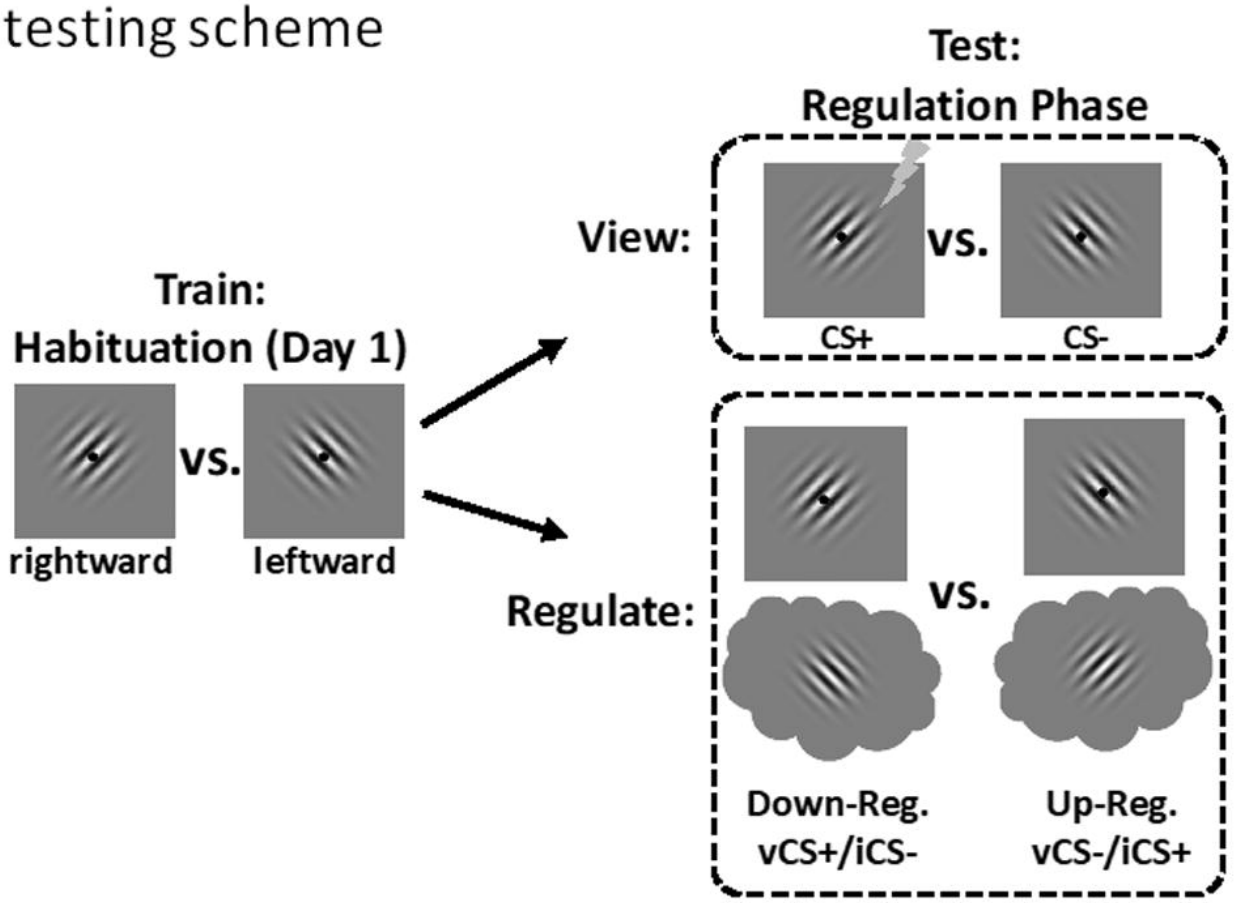

b. Exp. 2 visual cortex MVCC results

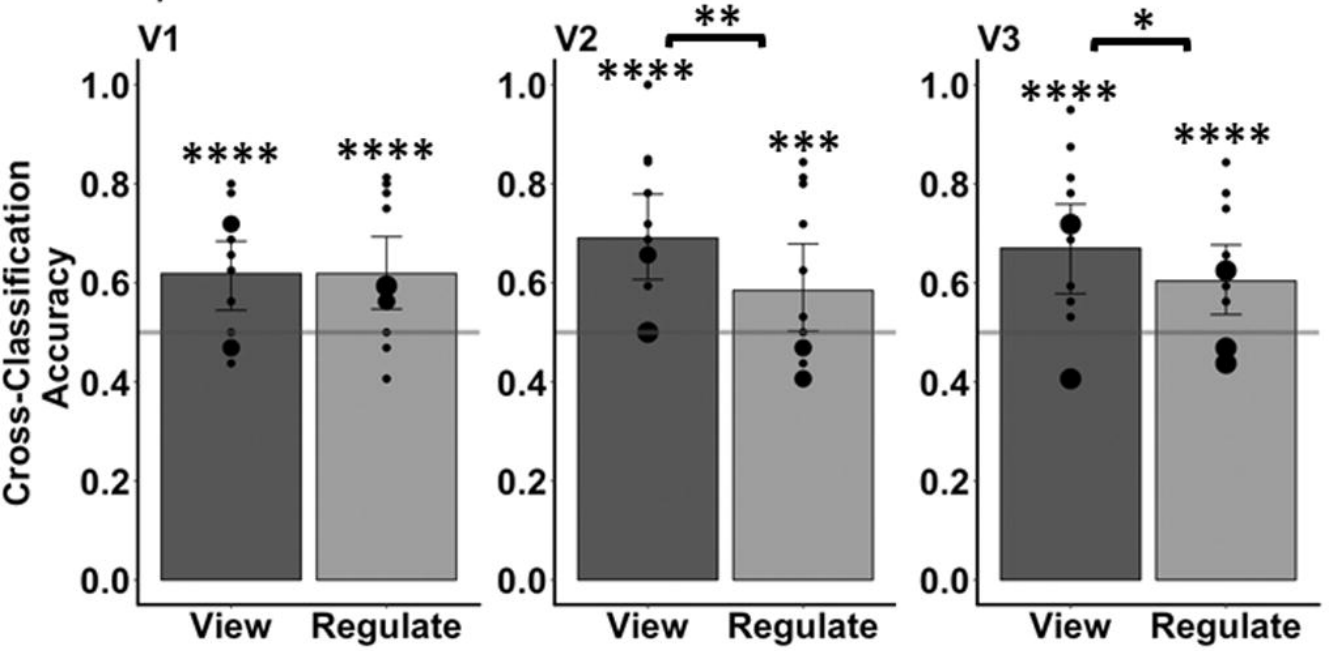

* $p < .05$ ** $p < .01$

*** $p < .001$ **** $p < .0001$

a. Exp. 2 amygdala MVCC training and testing scheme

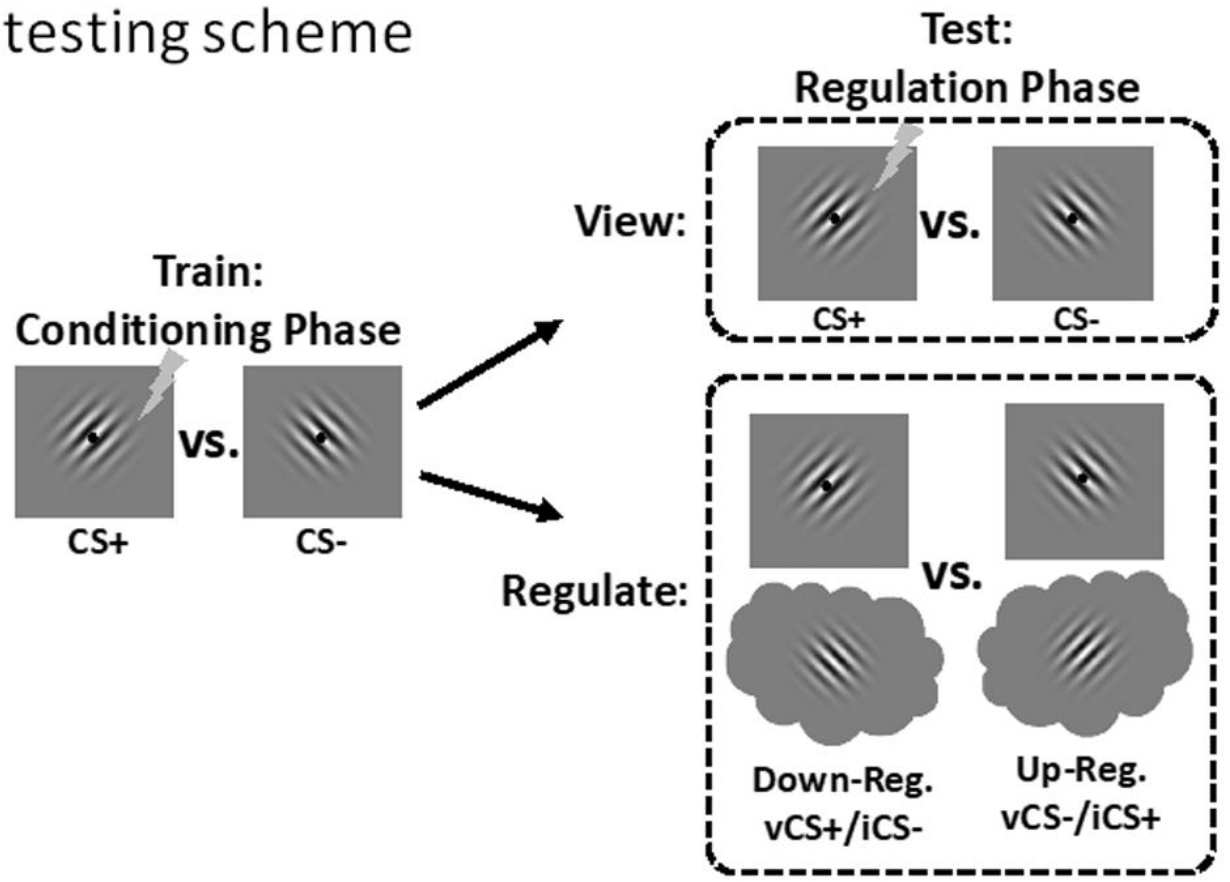

b. Exp. 2 amygdala MVCC results

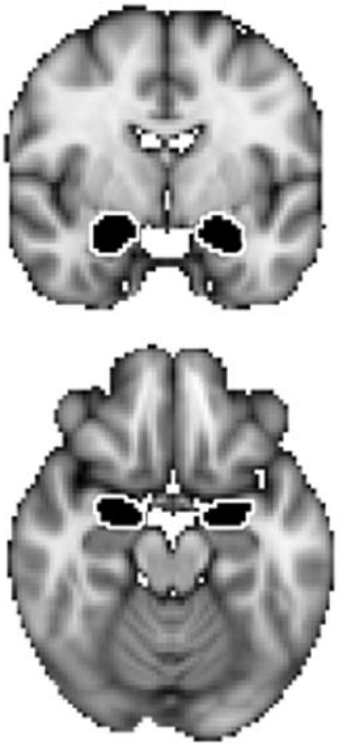

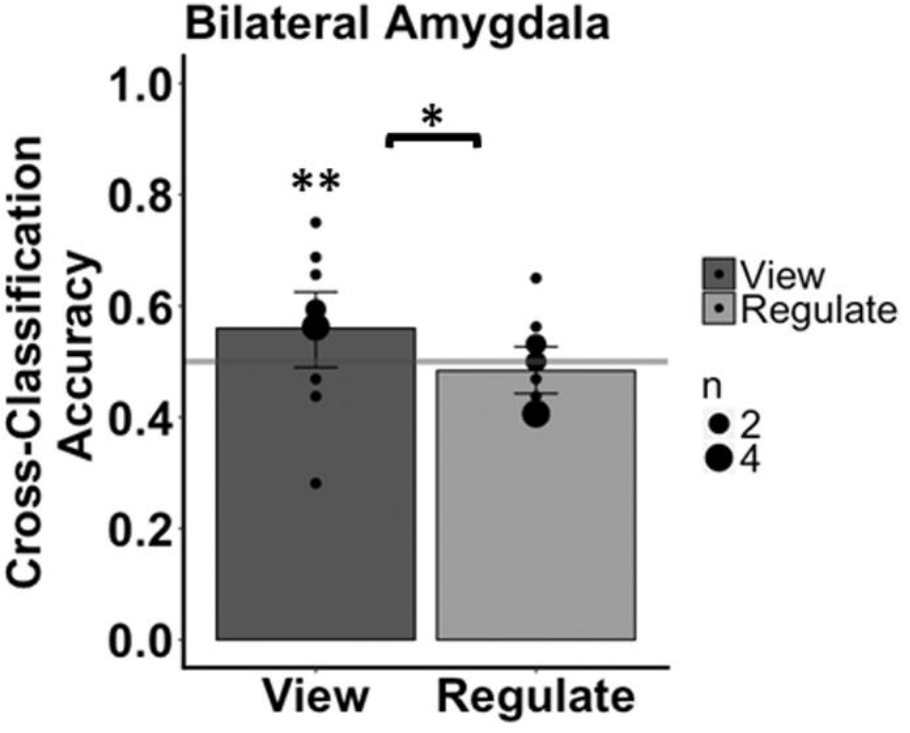

* $p < .05$ ** $p < .01$

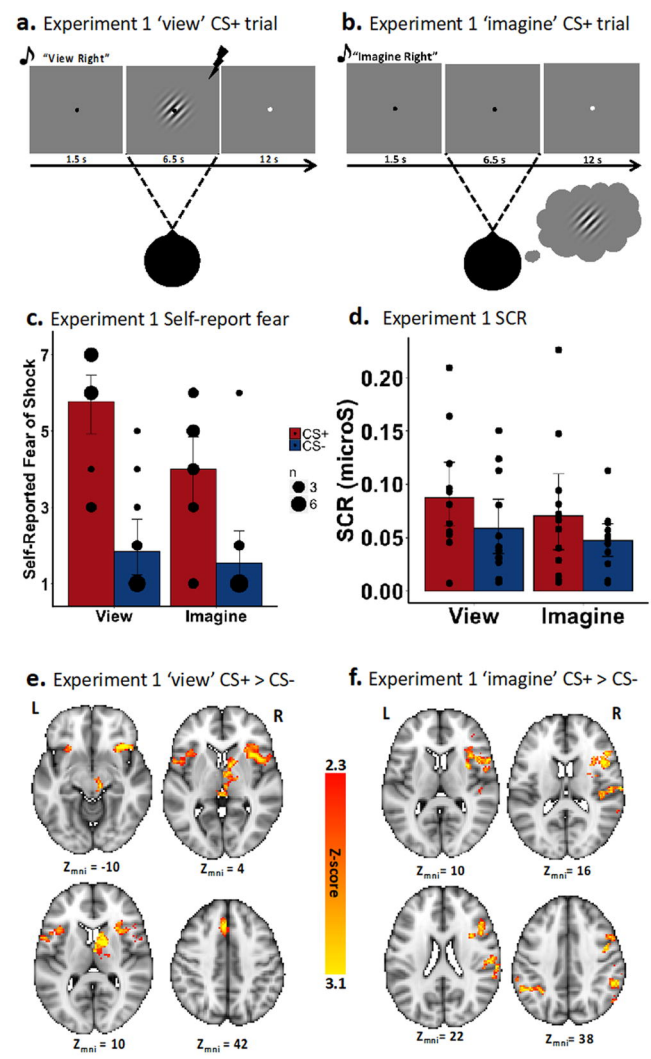
a. Experiment 1 'view' CS+ trial
"View Right"
1.5 s
6.5 s
12 s
b. Experiment 1 'imagine' CS+ trial
"Imagine Right"
1.5 s
6.5 s
12 s
c. Experiment 1 Self-report fear
Self-Reported Fear of Shock
7
5
3
1
CS+
CS-
n
3
6
View
Imagine
d. Experiment 1 SCR
SCR (microS)
0.20
0.15
0.10
0.05
0.00
View
Imagine
e. Experiment 1 'view' CS+ > CS-
L
R
Zmni = -10
Zmni = 4
Zmni = 10
Zmni = 42
2.3
Z-score
3.1
f. Experiment 1 'imagine' CS+ > CS-
L
R
Zmni= 10
Zmni= 16
Zmni= 22
Zmni= 38